Combustion Behind Shock Waves

Sandeep Singh, Daniel Lieberman, and Joseph E. Shepherd[1]

Graduate Aeronautical Laboratories,
California Institute of Technology, Pasadena, CA 91125, USA

October 13, 2003 *Revised Oct 22, 2003*

Abstract

Laminar hydrocarbon flames, which have adiabatic flame speeds on the order of a meter per second, are conventionally described by a leading convective-diffusive zone followed by an energy-releasing reactive-diffusive region. On the other hand, combustion induced by a strong shock wave is typically modeled as a convective-reactive balance with negligible diffusion, which may be called a convective explosion or fast flame. The transition between these two modes of combustion is an important issue in flame acceleration and transition from deflagration to detonation. In this study, we examine the range of pre-mixed combustion modes possible behind shock waves through numerical solutions of the one-dimensional, steady reactive Navier-Stokes equations with a detailed chemical reaction mechanism for stoichiometric methane-air mixtures. Shock Mach numbers ranging between one and the Chapman-Jouguet (CJ) value, a maximum of about five for typical fuel-air mixtures, are considered. The mixture examined in this study is stoichiometric methane-air. Two issues are considered in depth; one is the transition from diffusion-controlled to diffusionless combustion when the combustion wave speed is specified; the other is the question of the existence of a well-defined adiabatic flame speed behind a strong shock wave.

1 Introduction

The present study addresses two issues in high-speed combustion of pre-mixed gases. The first issue is the role of diffusion in detonation propagation, and the second is the existence of a well-defined adiabatic burning velocity in high-temperature mixtures. Our approach to these problems is numerical and is based on computing steady combustion wave structure using realistic thermochemistry, transport, and a detailed chemical kinetic model of methane-air combustion. A pseudo-time-stepping method with an adaptive spatial grid and finite-difference approximations to spatial derivatives is used to integrate the conservation equations until a steady-state, steady-flow solution is reached. We have examined the solution regimes as a function of the initial conditions, focusing on the effect of initial temperature and flow velocity.

The motivations for the present study come from a desire to understand the role of diffusion flames and diffusive transport processes in high-speed combustion and detonations. On a fundamental level, high-speed combustion waves can arise in a wide variety of combustion situations due to role of temperature gradients and hot spots in the ignition process, see for example, the recent discussion of Gu et al. (2003). One application is to high-speed turbulent flame propagation in tubes with obstacles, see for example, Knystautas et al. (1998). Flame speeds

[1]Corresponding author. E-mail: jeshep@galcit.caltech.edu. Tel: 626 395 3283.

can be as high as 1000 m/s before transition to detonation takes place. Another application is the structure of highly-unstable detonation fronts that have been observed (Pintgen et al., 2003, Austin, 2003) in fuel-air mixtures with large effective activation energies. Our goal is to understand the range of mechanisms in high-speed combustion that takes place behind shock fronts. Our initial study concerns strictly one-dimensional waves, although the ultimate application is to multi-dimensional flow that occurs in flame acceleration, transition to detonation, and detonation propagation.

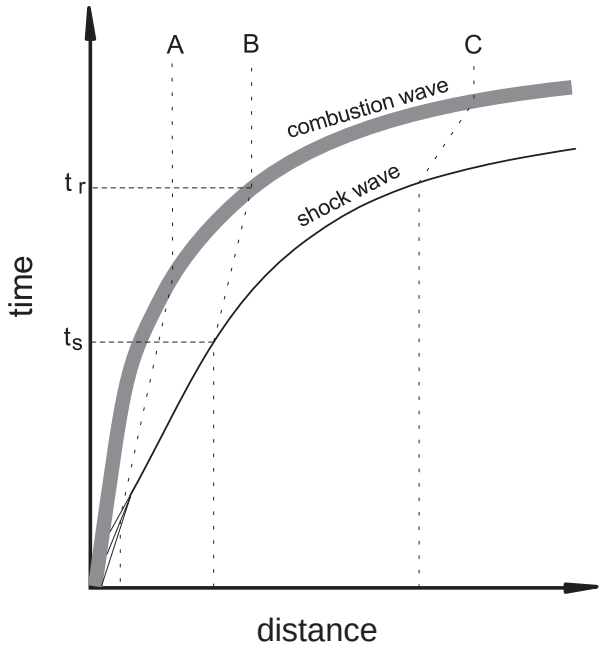

Figure 1: Schematic space-time diagram illustrating a combustion wave following an unsteady shock

In these high-speed combustion situations, there is a leading shock front created by the rapid volume generation of the following combustion process, see Fig. 1. If we consider the entire spectrum of combustion events that can occur in a mixture, starting from low-speed flames and ending with detonations, then the leading shock speed varies from Mach 1 up to the CJ value, between Mach 4 and 7. Most of the situations we are considering are intrinsically non-steady, with a lower-speed flame following a higher-speed shock wave, as shown in particle path A in Fig. 1. As long as the temperature behind the shock front is not too high, then we expect that the combustion wave behind the shock will have to be initiated externally and subsequently move relative to the flow at speeds less than 10 m/s, typical of diffusion-controlled combustion. As the shock speed and post-shock temperature increase, then the possibility exists that the shock wave sets up an induction time sufficiently short that the combustion wave propagates at high speed along a reaction locus (thick shaded curve in Fig. 1) that is determined by the reaction rates and the time history of the shock speed. Particle path B in Fig. 1 is representative of this situation. These high-speed waves are related to the spontaneous flame concept of Zel'dovich (1980), and are termed a "fast flame" by Clarke (1989). As the flame speed increases, simple physical arguments suggest that the role of diffusional transport

will diminish relative to convection. Eventually, for high enough flame speeds, diffusion will be negligible. Finally, when the induction time is sufficiently short, the reaction zone will closely follow the shock with a detonation-like structure, illustrated by particle path C in Fig. 1.

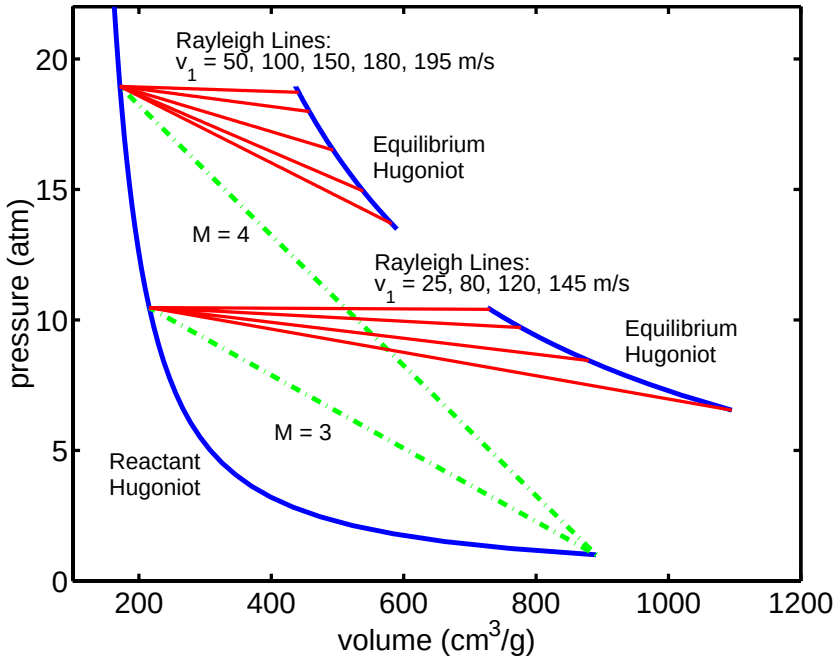

Figure 2: Pressure-volume plot for a reactant mixture of stoichiometric methane-air at a temperature and pressure of 300 K and 1 atm, respectively. Shock adiabats for Mach numbers 3 and 4 are depicted. Rayleigh lines starting from the post-shock states and ending at the equilibrium Hugoniots are also depicted for varying burning velocities.

An alternate way to visualize these processes is in the pressure-volume plane shown in Fig. 2. In this plot, as in the remainder of the paper, we have used a stoichiometric mixture of methane-air at a temperature of 300 K and pressure of 1 atm to illustrate the situation we are considering. Upstream of the combustion wave, we suppose that there is a shock wave propagating with a Mach number $M = U_{shock}/c_0$ into the stationary reactants, where U_{shock} is the shock speed and c_0 is the sound speed in the quiescent reactants. The properties behind the shock wave are computed using realistic thermochemistry and the shock jump conditions with a frozen composition. Figure 3 shows the computed post-shock temperature as a function of shock Mach number, and Fig. 4 shows the computed post-shock pressure as a function of shock Mach number. The locus of post-shock states is labeled as the reactant Hugoniot in Fig. 2. Two representative post-shock states for $M = 3$ and $M = 4$ are shown with the associated Rayleigh lines connecting the initial and post-shock states.

For two of the post-shock states in Fig. 2, we show Rayleigh lines that are labeled by the corresponding speed of the combustion wave following the shock. These Rayleigh lines terminate on an equilibrium (product) Hugoniot which is specific to each post-shock state. The nearly horizontal Rayleigh lines correspond to the diffusion-controlled flame solutions. The temperature and species profiles of one such solution are depicted in Figs. 5 and 6, respectively.

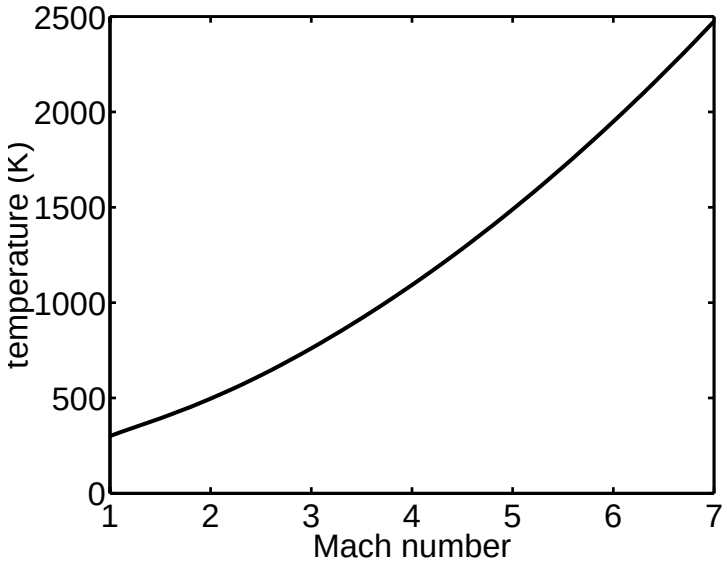

Figure 3: Post-shock temperature vs. shock Mach number for stoichiometric methane-air mixture at a pre-shock temperature and pressure of 300 K and 1 atm, respectively. Post-shock temperature increases with the shock Mach number along the reactant Hugoniot.

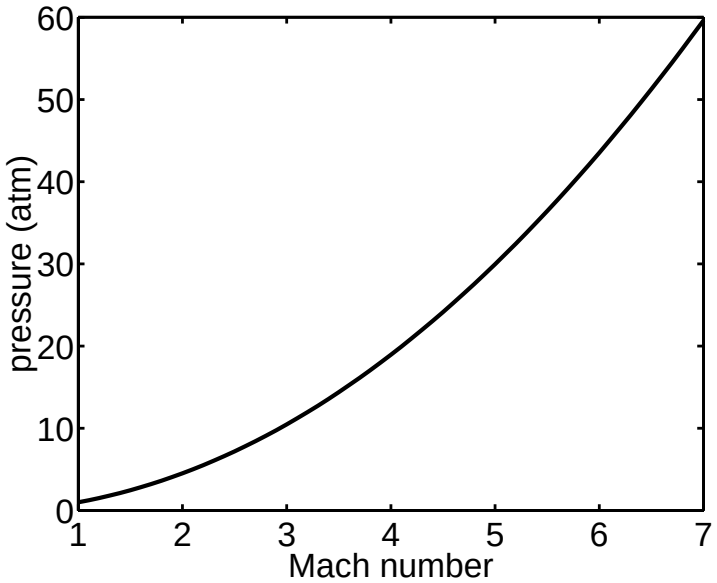

Figure 4: Post-shock pressure vs. shock Mach number for stoichiometric methane-air mixture at a pre-shock temperature and pressure of 300 K and 1 atm, respectively. Post-shock pressure increases with the shock Mach number along the reactant Hugoniot.

The steeper Rayleigh lines represent diffusionless solutions. The limiting case of these diffusionless solutions is the classical Zel'dovich-von Neumann-Döring (ZND) model (Fickett and Davis,

1979) of ideal detonation structure. The temperature and species profiles of a detonation case are depicted in Figs. 7 and 8. This particular case is for a slightly "overdriven", i.e., $M > M_{CJ}$ wave with a Mach number of 5.2. The leading shock wave is located at $x = 0$ in these simulations, off-scale to the left on the plots. The CJ solution for this mixture corresponds to a shock Mach number of 5.11 and a combustion wave velocity of 1809 m/s. The equivalent combustion wave velocity for this case is 300 m/s, which is the velocity of the flow relative to the shock. By contrast, the adiabatic diffusion flame solutions have combustion wave speeds of about 6 m/s at comparable thermodynamic conditions.

The temperature profiles for the flame and the detonation are similar in shape but the initial and final temperatures in the detonation are about 1000 K higher in the detonation than in the flame case. This reflects the essential difference between flames and detonations; the chemical reaction in the detonation case is initiated by high-temperature reactions behind the shock front while the chemical reaction in flames is initiated in the low-temperature pre-heat zone by diffusion of species and energy forward from the high-temperature products. The species profiles in the detonation case appear to increase much more rapidly with distance at the end of the induction period than at the end of the pre-heat zone for the flame case. However, the flame is actually thinner ($\delta = 1$ mm) than the detonation ($\Delta = 15$ mm) because the flow is much faster in the detonation case and also radical diffusion is more effective in initiating combustion as compared to the adiabatic chain branching that occurs in the detonation induction zone. The spatial extent (0.5 mm) of the region of the rapid transition in species concentration is comparable in both cases.

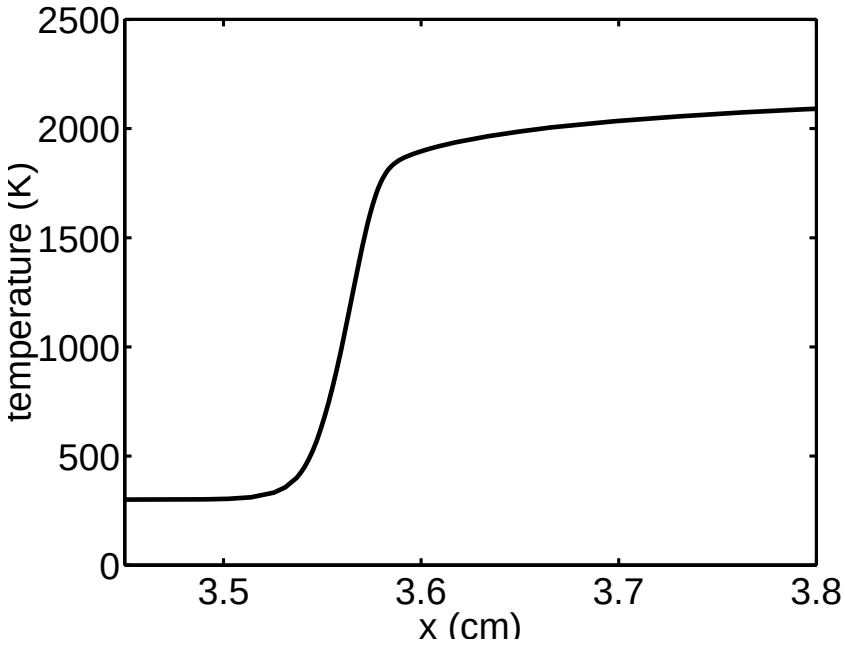

Figure 5: Temperature profile of a one-dimensional, pre-mixed, adiabatic, stoichiometric methane-air flame with the reactants at a temperature and pressure of 300 K and 1 atm, respectively.

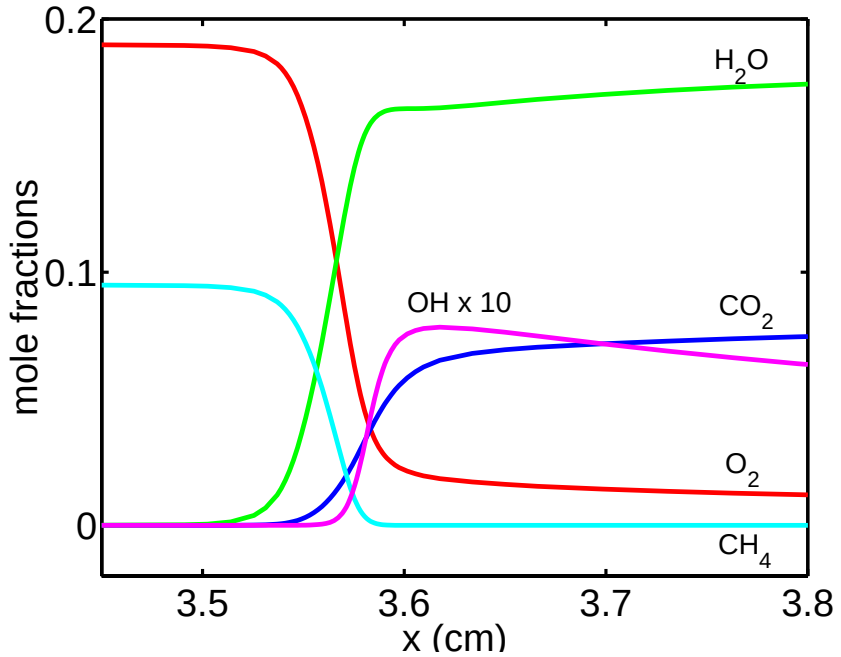

Figure 6: Species profile of a one-dimensional, pre-mixed, adiabatic, stoichiometric methane-air flame with the reactants at a temperature and pressure of 300 K and 1 atm, respectively.

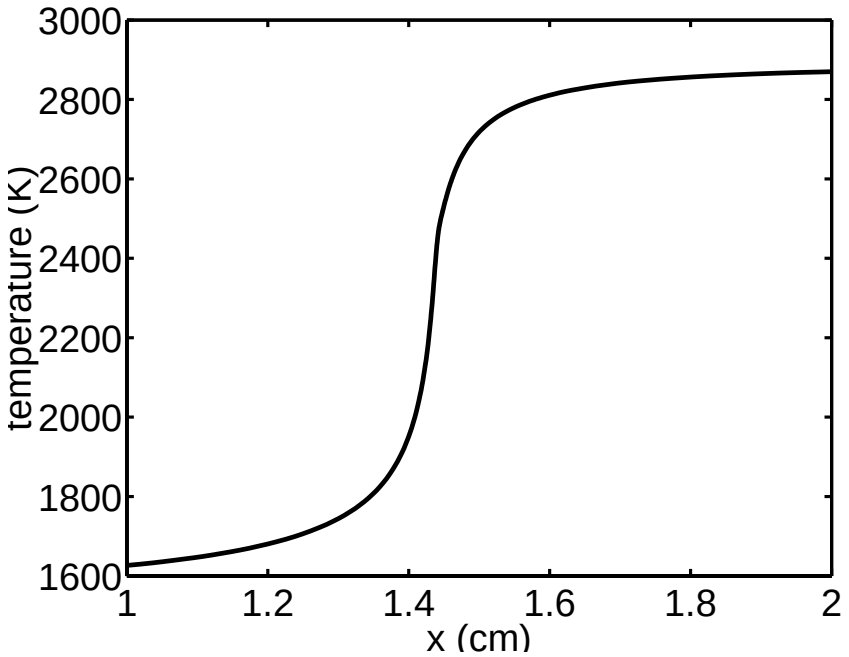

Figure 7: Temperature profile of a ZND model for a Mach 5.2 shock in a stoichiometric methane-air mixture at a temperature and pressure of 300 K and 1 atm, respectively.

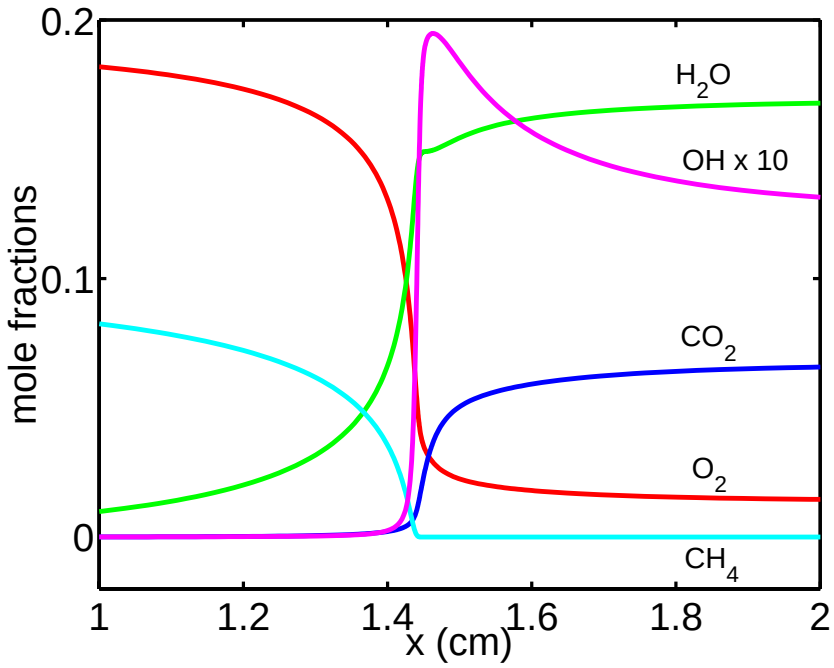

Figure 8: Species profile of a ZND model for a Mach 5.2 shock in a stoichiometric methane-air mixture at a temperature and pressure of 300 K and 1 atm, respectively.

Existence of Adiabatic Burning Velocity

Diffusion is an essential process in low-speed combustion, both laminar and turbulent (Peters, 2000, Liñań and Williams, 1993). A balance between convection, diffusion, and reaction determines the structure and speed of a a freely-propagating adiabatic flame. Computing steady-state, steady-flow flame structure and the associated burning velocity has become a standard numerical tool for the combustion analyst. For freely-propagating flames, the flow is considered to be adiabatic and effectively infinite in extent. In actual implementation, a finite length computational domain is used and the adiabatic burning velocity is computed as an eigenvalue by anchoring the flame to a location x_{fix} such that the temperature T_{fix} at that location remains fixed (Kee et al., 1985). An example is shown in Fig. 5 of the temperature profile for an adiabatic flame (stoichiometric methane-air, $M = 1$, i.e., $T_1 = 300$ K and $P_1 = 1$ atm) computed by the algorithm described in Section 4. The associated species profiles are shown in Fig. 6. As shown, the spatial gradients in temperature and species amount are small at the upstream boundary $x = 0$, off scale to the left on these plots. In this case, the values used for the computation are $x_{fix} = 3.5$ cm and $T_{fix} = 400$ K.

A key assumption made in carrying out adiabatic burning velocity computations is that it is always possible to find a range of parameters x_{fix} and T_{fix} for a given reactant mixture such that the computed burning velocity is relatively independent of these choices. In that situation, we can speak of "the adiabatic burning velocity" as a single, well-defined quantity. In fact, the combustion literature contains a large number of papers describing such simulations for many different fuel-oxidizer mixtures and initial conditions, indicating that this assumption is widely found or assumed to be valid. In the present study, we are able to obtain meaningful solutions for adiabatic burning velocity for post-shock states corresponding to shock Mach numbers of up to $M = 5$ which is associated with an initial temperature of 1490 K. For values of $M > 5$, as discussed in more detail later, we could not obtain solutions for adiabatic flames which had an obviously unique burning velocity.

A simple explanation of the limitations in obtaining an adiabatic laminar flame speed can be given in terms of the competition of reaction processes upstream of the flame with those within the flame. This possibility arises because at sufficiently high reactant temperatures, the reactant mixture can undergo adiabatic explosion without the diffusion of species and energy between the hot products and the reactants, which is the mechanism for reaction initiation in low-temperature reactant mixtures entering the flame zone. This means that at high initial temperatures, the reaction rates will be high enough that x_{fix} cannot be arbitrarily chosen. For any reactive mixture, we can define an adiabatic explosion or induction time t_i that strongly decreases as the reactant temperature is increased. When the residence time x_{fix}/v_a, where v_a represents the adiabatic burning velocity, exceeds the induction time, an adiabatic flame solution will no longer be possible. This is because the reactant mixture will adiabatically explode in the region upstream of the location x_{fix} where the combustion wave has been anchored, resulting in an upper bound for x_{fix}. At the same time, there is a lower bound for x_{fix}, which is between two and three times the flame thickness δ, such that there is no energy and mass loss at the upstream boundary $x = 0$. The adiabatic burning velocity and flame thickness determine the bounds for x_{fix}, and their variation with shock Mach number is depicted in Figs. 9 and 10, respectively. The flame thickness shown here is based on the maximum slope of the temperature profile

$$\delta = \frac{T_{max} - T_{min}}{dT/dx|_{max}} \tag{1}$$

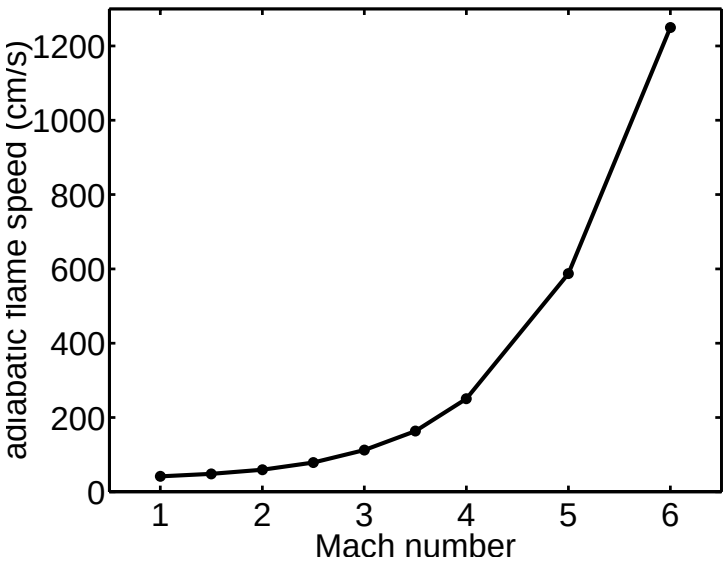

Figure 9: Adiabatic burning velocity for varying post-shock conditions vs. the corresponding shock Mach number.

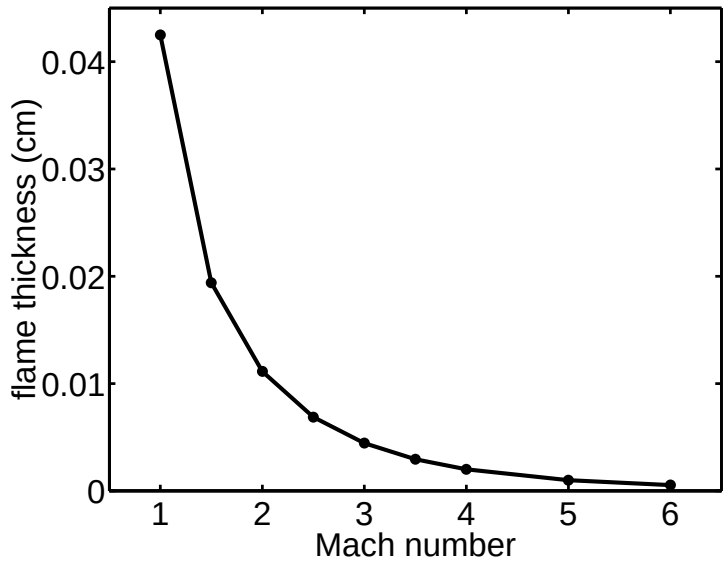

Figure 10: Adiabatic flame thickness for varying post-shock conditions vs. the corresponding shock Mach number.

We will find that the mechanisms discussed here yield an upper bound for the shock Mach numbers for which we can find solutions to the adiabatic burning velocity problem.

Transition in Combustion Mechanism with Wave Speed

Detonations are in a combustion regime at the opposite end of the spectrum from laminar diffusion flames. Detonations nominally propagate with speeds between 1500 and 3000 m/s and the associated combustion wave speed is between 200 and 500 m/s. All conventional analyses take as an initial assumption that diffusive processes are irrelevant to the structure and speed of propagation of detonation waves (Liñań and Williams, 1993, See pp. 100-101). The basis of this assumption is not clearly articulated in the combustion literature. Although the role of diffusion in detonation has been examined by a number of researchers (Fickett and Davis, 1979, See p. 192), the conclusions appear to be contradictory (Fickett and Davis, 1979, See p. 199) with some analyses and numerical simulations indicating that diffusion has a substantial effect on detonation structure while others do not. Diffusion has been used in some studies (Singh et al., 2001) as a means of regularizing numerical solutions for propagating detonations, and the role of diffusion has been the subject of numerous mathematical investigations (Chen and Wagner, 2003, for example) into the formal question of the existence of solutions to the reactive Navier-Stokes equations. Setting aside mathematical issues of uniqueness and existence, the issue for physical scientists and engineers is: Can reliable computations of detonation structure be made without considering diffusion? From a physical point of view, Clarke's analyses (Clarke, 1983, 1989) of the role of diffusion in high-speed combustion clearly indicates that diffusion cannot be a significant factor in determining detonation structure when realistic values of transport coefficients and reaction rates are used in one-dimensional analyses. We will see that this is supported by the numerical analyses we have carried out but that this conclusion may have to be reconsidered for multi-dimensional detonations with highly unstable fronts.

The conventional approach (Fickett and Davis, 1979, Chap. 5) is that balance between convection and reaction, which is the essence of the ZND model, is considered to completely determine the structure of an ideal detonation wave. Further, the speed is determined not by the balance in processes but rather by the thermochemistry and the CJ hypothesis - the flow at the end of the reaction zone is sonic relative to the leading shock wave. In essence, the high-speed combustion process is a convected adiabatic explosion. Solutions are possible for a wide range of combustion wave speeds as long as singularities do not appear in the reaction zone, which is sometimes known as the generalized CJ condition. The CJ solution is singled out because this case corresponds to what is observed in the laboratory experiments with self-supporting waves, and can be justified by appealing to the isolating nature of the sonic surface.

A ZND-like combustion wave solution is limited to high temperatures since below some minimum temperature, the reaction rates are so slow that it is not possible to obtain adiabatic explosions in any sensible time. The induction time, computed assuming a constant pressure explosion process, as a function of shock Mach number for our example case, is shown in Fig. 11. Obviously, for shock Mach numbers less than 3, it is difficult to conceive of adiabatic explosion processes in ordinary laboratory situations and the induction time exceeds 1 s. In these cases, the only possibility for obtaining propagating combustion waves is to have continuous initiation by diffusion of hot products and reactive intermediates from downstream into the unreacted mixture upstream. So we expect that, behind weak shocks, we will have diffusion-controlled combustion and behind strong shocks, diffusionless adiabatic explosion waves. Setting aside the issue of how such combustion waves are set up, we can consider the mode of combustion behind a shock of given strength as a function of wave speed ranging between the two extremes of 1-10 m/s for laminar flames to the 300 m/s for ZND-like combustion waves. As pointed out earlier,

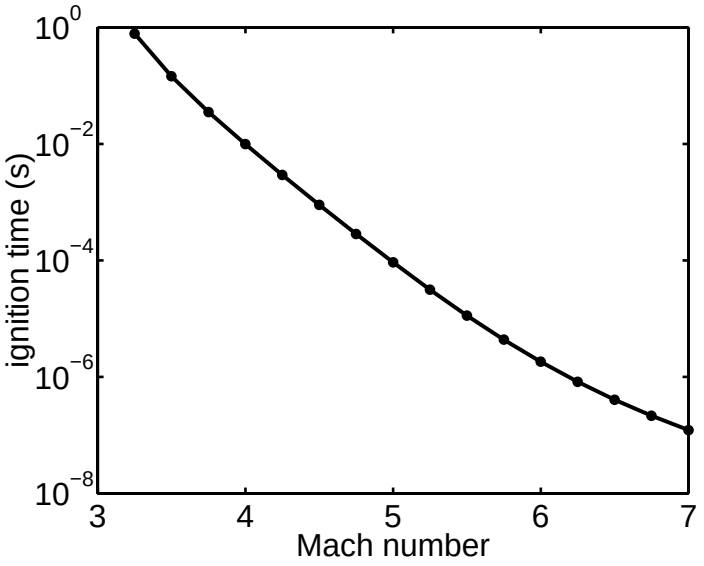

Figure 11: Induction time for post-shock states vs. shock Mach number for stoichiometric methane-air. This is defined here as the time required for the temperature to reach 100 K above the starting temperature.

these are non-steady solutions since the leading shock and combustion wave necessarily travel at different velocities except in the special case of the ZND solution with wave speeds equal to or greater than the CJ velocity.

What types of processes occur in combustion waves that propagate with intermediate velocities? Clarke, Kassoy, and co-workers have done extensive analysis (summarized in Clarke, 1989) on regime intermediate between laminar flames and detonations. Clarke has used asymptotic analysis and distinguished limit considerations to show that diffusion becomes negligible at finite flow speeds that are quite modest in comparison to detonation velocities. Since these studies are carried out with asymptotic methods, precise bounds on the behavior are not established and it is unclear how to apply these results to cases with detailed chemistry. We carry out computations for our example stoichiometric methane-air mixture using a detailed reaction mechanism and show exactly how this transition comes about. Our numerical studies confirm the gradual transition from diffusion-controlled to diffusionless combustion as the combustion wave speed is increased. We show that in addition to the considerations given by Clarke, it is essential to consider the effect of post-shock temperature, as discussed previously in connection with the issue of the existence of laminar flame solutions.

2 Problem Description

The schematic for a combustion wave trailing a shock wave is shown in Fig. 12. In a non-steady regime, the two waves propagate at different speeds. The stationary reactant mixture is first shocked and then a combustion wave burns the warm reactants and generates hot products.

The steady combustion wave is computationally modeled as shown in Fig. 13, which also shows the velocities of the warm shocked reactants and the hot products in a wave-fixed coor-

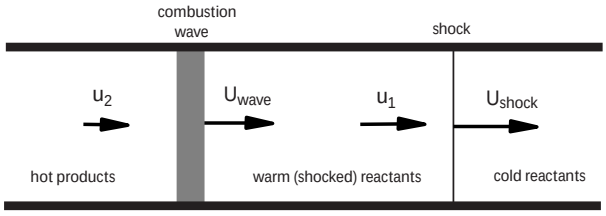

Figure 12: Schematic of the physical problem for study of combustion behind shock waves.

dinate system. In our study, these waves are modeled in one spatial dimension.

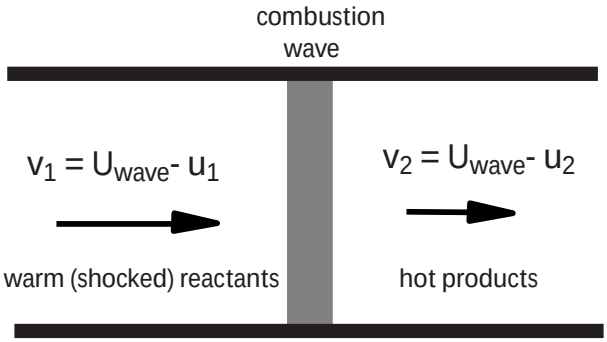

Figure 13: Schematic of the computational domain for analysis of the steady combustion wave.

3 Governing Equations

One-dimensional steady, laminar combustion is governed by the reactive Navier-Stokes equations (Kee et al., 2003). In our study, we have considered the following approximate version of this model consisting of $N+4$ equations for an ideal mixture of N chemical species:

$$\frac{\mathrm{d}\mathcal{M}}{\mathrm{d}x} = 0, \tag{2}$$

$$\frac{\mathrm{d}}{\mathrm{d}x}\left(p + \frac{\mathcal{M}^2}{\rho}\right) = 0, \tag{3}$$

$$\underbrace{-\mathcal{M}\frac{\mathrm{d}T}{\mathrm{d}x}}_{\text{tconv}} \underbrace{+\frac{\mathcal{M}}{\rho c_p}\frac{\mathrm{d}p}{\mathrm{d}x}}_{\text{tpress}} \underbrace{-\frac{1}{c_p}\frac{\mathrm{d}J^q}{\mathrm{d}x}}_{\text{tcond}} \underbrace{-\frac{1}{c_p}\sum_{k=1}^{N} J_k^m c_{pk}\frac{\mathrm{d}T}{\mathrm{d}x}}_{\text{tdiff}} \underbrace{-\frac{1}{c_p}\sum_{k=1}^{N}\dot{\omega}_k h_k W_k}_{\text{treac}} = 0, \tag{4}$$

$$\underbrace{-\mathcal{M}\frac{\mathrm{d}Y_k}{\mathrm{d}x}}_{\text{yconv}} \underbrace{-\frac{\mathrm{d}J_k^m}{\mathrm{d}x}}_{\text{ydiff}} \underbrace{+\dot{\omega}_k W_k}_{\text{yreac}} = 0, \qquad k = 1, \ldots, N, \tag{5}$$

$$p = \rho \Re T \sum_{k=1}^{N} \frac{Y_k}{W_k}, \tag{6}$$

where the $N + 4$ dependent variables are ρ, p, T, $\mathcal{M}$, and Y_k ($k = 1, \ldots, N$, $\sum_{k=1}^{N} Y_k = 1$), which represent density, pressure, temperature, mass flow rate ($= \rho v$), and the N species mass fractions, respectively. The independent space variable is represented by x. Equations (2-5) describe the conservation of mass, momentum, energy, and species at steady-state, and are derived from the steady-state reactive Navier-Stokes equations (Kee et al., 2003) by neglecting the effects of viscosity. Equation (6) is the ideal gas equation of state. The molecular weight of species k is represented by W_k, and the universal gas constant is represented by $\Re$. Since all the species are assumed to be ideal gases, the specific heat at constant pressure of species k, c_{p_k}, is a function of temperature alone. The mass-averaged specific heat at constant pressure for the fluid mixture is given by $c_p = \sum_{k=1}^{N} Y_k c_{p_k}$. The specific enthalpy of species k is given by $h_k = h_k^\circ + \int_{T_\circ}^{T} c_{p_k}(\hat{T}) d\hat{T}$, where h_k° is the standard enthalpy of formation per unit mass of species k at the standard temperature of $T_\circ = 298$ K. The thermodynamic database of Kee et al. (1987) and the gas phase kinetics package of Kee et al. (1989) are used to compute c_{p_k}, c_p, and h_k.

The molar rate of production of species k, $\dot{\omega}_k$, is given by the law of mass action with Arrhenius kinetics

$$\dot{\omega}_k = \sum_{j=1}^{J} a_j T^{\beta_j} \exp\left(\frac{-E_j}{\Re T}\right) \left(\nu''_{kj} - \nu'_{kj}\right) \prod_{i=1}^{N} \left(\frac{\rho Y_i}{W_i}\right)^{\nu'_{ij}}, \tag{7}$$

where J is the number of elementary reactions in the N species reaction mechanism. The constant parameters a_j, β_j, and E_j represent the kinetic rate constants of reaction j, the temperature dependence exponent of reaction j, and the activation energy of reaction j, respectively. The stoichiometric coefficients of species k on the reactant and product sides of the elementary reaction j are represented by ν'_{kj} and ν''_{kj}, respectively. The subroutines in the gas phase kinetics package are used to compute $\dot{\omega}_k$ with all the parameters provided by a detailed reaction mechanism.

The thermal conduction flux is given by Fourier's law

$$J^q = -\lambda \frac{\mathrm{d}T}{\mathrm{d}x}, \tag{8}$$

where λ is the mass averaged thermal conductivity of the fluid mixture, which depends on temperature, pressure, and composition of the fluid mixture. The energy flux due to mass diffusion is given by the fourth term in the energy conservation Eq. (4), while the energy flux due to the Dufour effect has been neglected.

The mass diffusion flux is given by Fick's law

$$J_k^m = -\rho \mathcal{D}_k \frac{W_k}{\overline{W}} \frac{\mathrm{d}X_k}{\mathrm{d}x} + \rho Y_k V_c, \qquad V_c = \sum_{k=1}^{N} \mathcal{D}_k \frac{W_k}{\overline{W}} \frac{\mathrm{d}X_k}{\mathrm{d}x}, \tag{9}$$

where $\mathcal{D}_k$ is the mass averaged diffusion coefficient of species k in the fluid mixture, which also depends on temperature, pressure, and composition of the fluid mixture. The mass averaged molecular weight of the fluid mixture is given by $\overline{W} = 1/\sum_{k=1}^{N}(Y_k/W_k)$, and the mole fraction of species k is given by $X_k = Y_k \overline{W}/W_k$. A correction diffusion velocity, V_c, is added to the mass

diffusion flux such that $\sum_{k=1}^{N} J_k^m = 0$. Mass diffusion fluxes due to pressure gradients, temperature gradients, and external forces have been neglected. The gas phase transport package (Kee et al., 1986) is used to compute λ and $\mathcal{D}_k$. Finally, the local flow velocity can be obtained by $v = \frac{\mathcal{M}}{\rho}$.

The inflow boundary conditions used for computing the steady combustion wave in the configuration depicted in Fig. 13, is given

$$\mathcal{M} = \mathcal{M}_1, \qquad p = p_1, \qquad T = T_1, \qquad Y_k = Y_{k1},\ k = 1, \ldots, N, \tag{10}$$

where the subscript 1 denotes the constant inflow state. The outflow boundary conditions are given by

$$\left.\frac{\mathrm{d}M}{\mathrm{d}x}\right|_2 = 0, \qquad \left.\frac{\mathrm{d}p}{\mathrm{d}x}\right|_2 = 0, \qquad \left.\frac{\mathrm{d}T}{\mathrm{d}x}\right|_2 = 0, \qquad \left.\frac{\mathrm{d}Y_k}{\mathrm{d}x}\right|_2 = 0,\ k = 1, \ldots, N. \tag{11}$$

The values of the individual terms with their signs in the energy conservation Eq. (4) and the species conservation Eq. (5) will be compared in Section 5. The terms representing convection, pressure gradient, thermal conduction, thermal diffusion due to mass diffusion, and reaction in the energy conservation equation have been labeled as tconv, tpress, tcond, tdiff, and treac, respectively. Similarly, the terms due to convection, mass diffusion, and reaction in the species conservation equation have been labeled as yconv, ydiff, and yreac, respectively. We have used these labels in the subsequent plots showing the variation of these terms in space for our steady-state flame solutions.

4 Numerical Method

In this section, we describe the computational algorithm used to solve Eqs. (2-6) for computing the steady combustion waves. We have retained the approximate momentum equation in order to properly describe high Mach number flows, this is the main difference between our equation formulation and the more standard approach of Kee et al. (1985). In the standard approach for solving the model equations of low Mach number steady flames, the momentum equation is reduced to the isobaric flow condition, P = constant. Eqs. (2-3) are integrated along with enforcing the following algebraic constraints

$$\mathcal{M} = \mathcal{M}_1, \tag{12}$$

$$p + \frac{\mathcal{M}^2}{\rho} = p_1 + \frac{\mathcal{M}_1^2}{\rho_1}, \tag{13}$$

respectively. The subscript 1 represents the inflow state of the reactant mixture flowing into the combustion wave as shown in Fig. 13.

Using spatial discretization and finite difference approximations for the spatial derivatives, Eqs. (4-5) and the associated boundary conditions can also be reduced to algebraic equations. Equations (2-6) coupled with the boundary conditions can be reduced to a set of algebraic equations which can be solved with a damped Newton solver. This methodology is used in the Kee et al. (1985) code. However, our practical experience is that convergence with the Newton solver can be difficult without a very good initial guess.

To avoid these convergence problems, we use a pseudo-time-stepping method to solve the differential Eqs. (4-5). It usually results in convergence even for poor initial guesses. The following partial differential equations are integrated till steady-state is achieved

$$\rho\frac{\partial T}{\partial \tau} = f_e(\rho, p, T, \mathcal{M}, Y_1, \ldots, Y_N), \tag{14}$$

$$\rho\frac{\partial Y_k}{\partial \tau} = f_{y_k}(\rho, p, T, \mathcal{M}, Y_1, \ldots, Y_N), \qquad k = 1, \ldots, N, \tag{15}$$

where τ is the pseudo-time variable, and the functions f_e and f_{y_k} represent the left hand sides of Eqs. (4-5). Using spatial discretization and central difference approximation for the spatial derivatives, Eqs. (14-15) are reduced to ordinary differential equations at each discrete spatial location. These equations, together with the algebraic Eqs. (12-13) and Eq. (6), are solved at each discrete spatial location in the interior of the computational domain. The algebraic equations resulting from the finite difference approximation of the boundary conditions coupled with the algebraic Eqs. (12-13) and Eq. (6) are solved at the boundaries. The coupled system of differential-algebraic equations is marched forward in time until the solution reaches steady state. Due to the existence of a wide range of time scales, the high-order implicit method of Petzold (1982) is used to carry out the solution. The solution is not time-accurate since only final steady-state solution is of interest.

The initial guess consists of reactants near the left inflow boundary and the hot equilibrium products near the right outflow boundary of the computational domain. The thermodynamic state and composition of the equilibrium products are found using the numerical code of Reynolds (1986). The regions between the reactants and products are initialized using a linear interpolation of the states in the reactants and products. The location of the computed flame front at steady-state varies with inflow velocity of the reactants. For this reason, the initial guess for the location of this linear flame front should be appropriately chosen for fast convergence.

An adaptive gridding procedure similar to that employed by Kee et al. (1985) is used to resolve the rapid spatial variations in the solution. The model equations are first solved on a coarse mesh. Additional grid points are then added in regions of high gradients and curvatures. A new grid point is added between two grid points if the spatial gradient and curvature of the solution between the two old grid points do not satisfy pre-assigned tolerances. The initial guess for the new refined mesh is obtained by linear interpolation of the solution from the old coarser mesh. The model equations are then re-solved on the refined mesh. The refinement and subsequent re-solving of the model equations on the refined grids is repeated until the pre-assigned tolerances for the solution gradient and curvature are achieved. Since this grid refinement procedure results in non-uniform spacing of the grid points, a weighted central difference approximation is used for the spatial derivatives.

If the inlet mass flow rate, $\mathcal{M}_1$, of the reactant mixture is known, then the model equations can be solved as described above to obtain the flame structure. The computational algorithm can also be modified to obtain the intrinsic adiabatic flame speed for the reactant mixture at a certain temperature, pressure, and composition. In this case, $\mathcal{M}_0$ is treated as an unknown, and a temperature at a certain location within the flame structure is fixed as was done by Kee et al. (1985). This can be accomplished by replacing the discretized form of Eq. (14) for a certain grid point i by the following equation

$$T^i - T_{fix} = 0, \tag{16}$$

where T^i is the temperature at the grid point i, and T_{fix} is a constant temperature value. A suitable choice for $T_{fix} = T_1 + 100$ is 100 K more than the reactant mixture temperature. There are certain restrictions for the spatial location x^i or the grid point i where the temperature can be fixed, and those will be discussed later in Section 5. This procedure allows for computation of $\mathcal{M}_1$ as the unknown eigenvalue, which gives the adiabatic flame speed as $v_a = v_1 = \mathcal{M}_1/\rho_1$. In our study, both modes of computation of the flame structure are used.

4.1 Validation

We have used the GRI Mech 1.2 mechanism (Frenklach et al., 1995) and the standard databases for thermochemistry (Kee et al., 1987) and transport coefficients (Kee et al., 1986) in the present study. Extensive validation was done on laminar flame speed and shock tube induction time as part of the GRI Mech development process and the results are available on the GRI Mech web site (Frenklach et al., 1995). We have not repeated these standard validations here but have examined the issue of laminar flame speed dependence on initial temperature.

There have been a number of experimental studies on the dependence of flame speed on initial temperature and pressure. Early work is discussed in Gaydon and Wolfhard (1979, pp. 81-86) and data for methane-air mixtures by Dugger and Heimel are given. More recently, Mishra (2003) has numerically simulated methane-air flames up to an initial temperature of 600 K and compared his results with some data. Experimentally, Elia et al. (2001) have carried out extensive combustion bomb studies and developed a correlation for the dependence of burning velocity on pressure (0.75 to 70 atm) and temperature (298 to 550 K). Elia et al. (2001) have compared their results with earlier experimental studies and have shown that there are substantial differences between the results of various investigators at higher temperatures, particularly at elevated pressure.

We have compared our results with those of previous researchers in Fig. 14 for stoichiometric methane-air mixtures at 1 atm initial pressure and initial temperatures between 300 and 600 K. Our results agree very well with the correlation of Elia et al. (2001) and are higher than Mishra's computations and the data of Hill and Hung (1988), Stone et al. (1998), and Garforth and Rallis (1978). On the other hand, our results are lower than data of Andrews and Bradley (1972) and the results of Dugger and Heimel as cited by Gaydon and Wolfhard (1979, Fig. 4.9).

No data are available for temperatures above 550 K to validate our predictions for high temperatures behind shock waves but we can extrapolate the correlation of Elia et al. (2001) to get a notion of the comparison (see Fig. 15). It is apparent that much larger values of burning velocity are predicted by our computations than by the extrapolation of the correlation based on lower-temperature data. Without experimental data, it is not possible to judge the validity of the present simulations since they are just as reasonable an extrapolation of the data as is the correlation of Elia et al. (2001).

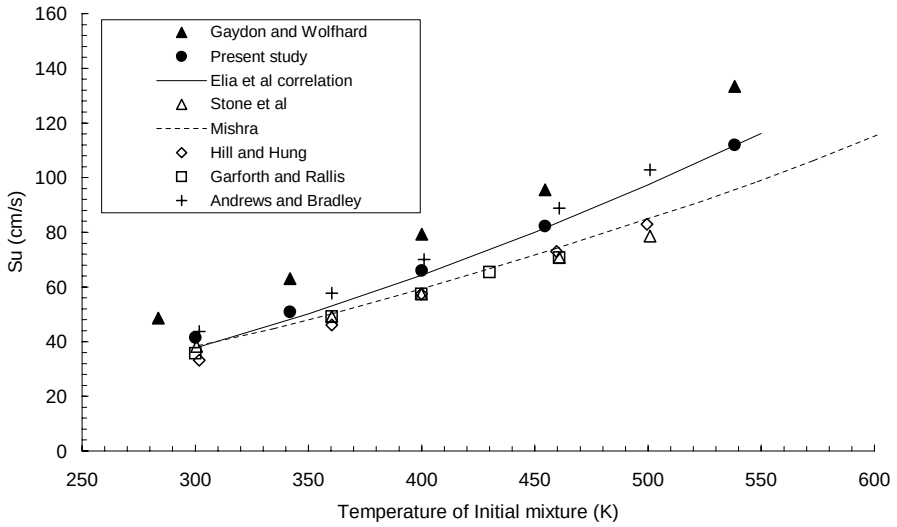

Figure 14: Dependence of laminar burning speed on initial temperature for stoichiometric methane-air mixtures at an initial pressure of 1 atm.

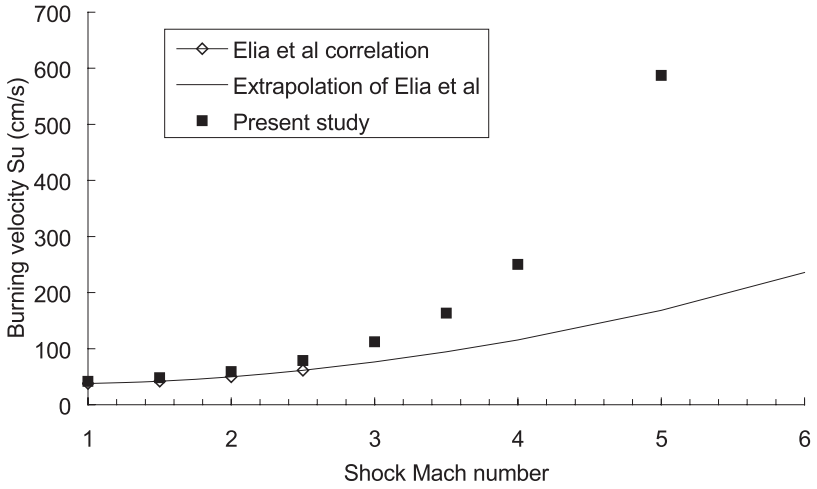

Figure 15: Dependence of laminar burning speed on shock Mach number for stoichiometric methane-air mixtures at an initial pressure of 1 atm and an initial temperature of 300 K.

5 Analysis and Results

The composition of the stoichiometric methane-air mixture that was used in this study is: X_{CH_4} = 0.095, X_{O_2} = 0.19, X_{N_2} = 0.715. The reaction mechanism GRI Mech 1.2 (Frenklach et al., 1995) was used; this involves 32 chemical species and 177 elementary reactions. We have carried out two types of simulations. First, in order to study the transition of a diffusion-controlled combustion wave or flame to convective explosion, we computed the flame structure for a fixed initial state varying the inlet mass flow rate. The reactant mixture is taken to be at the post-shock state of a Mach 5 shock with a pre-shock state of temperature 300 K and pressure 1 atm. Second, in order to study the existence of laminar flames behind shock waves we have computed the adiabatic flame speed for an initial state that corresponds to the post-shock conditions in non-reactive shock waves with shock Mach numbers between 1 and 6. Finally, in order to examine the dependence of the balance of transport processes within the flame, a separate set of computations of adiabatic flame speed was carried out for initial pressures between 1 and 100 atm for an initial temperature of 300 K.

5.1 Transition of Diffusion-Controlled Flame to Convective Explosion

Clarke (1983) was the first to describe the change in the dominant balance structure of combustion waves as the speed was increased from "low" to "high". His study was based on defining a local Damköhler number and indentifying several distinguished limits depending on the Mach number of the combustion wave. In our present numerical simulations, we clearly observe the essential results of his analysis which is that, at combustion wave Mach numbers that are large compared to the laminar burning value but small compared to one, the role of diffusion is neglible and flame becomes a convected explosion process.

Figures 16-19 depict the transition from the diffusion-controlled flame to the convective explosion as the combustion wave speed or the inflow velocity of the reactants is increased. Figure 16 depicts the variation in space of the magnitudes of the individual terms in Eq. (4) at an inflow velocity of v_1 = 2 m/s. In this case, there is a very small pre-heat zone where convection and diffusion balance each other and chemical reaction is negligible. This is followed by a region of thermal explosion where chemical reaction is predominantly balanced by diffusion, but the effects of convection are not negligible. The thermal explosion region consists of a small fast reaction region, where intermediate species are produced, followed by a longer slow reaction region where the recombination reactions occur to form hot products. Note that except for the pre-heat zone, there is always an interplay of the reaction, convection, and diffusion effects until equilibrium is reached, and we don't have a pure reaction-diffusion region where reaction is balanced only by diffusion. Figure 20 depicts the corresponding plot for the variation in space of the magnitude of the individual terms in the species balance equation. At such low speeds, which are below the adiabatic flame speed, there are mass and energy losses and the temperature and mass gradients are not small at the inflow computational boundary.

For comparison, Figs. 17 and 21 depict the energy balance terms and species balance terms, respectively, for an adiabatic flame for the same reactant mixture at the same post-shock state. The adiabatic flame speed is v_1 = 5.81 m/s. It can be deduced from Figs. 17 and 21 that energy and mass loss at the inflow computational boundary is negligible for this wave speed. This is because all solution gradients become negligible at the inflow boundary and therefore, convection and diffusion also become negligible there. In other respects, the plots are very

similar to the previous case of $v_1 = 2$ m/s. There is a pre-heat zone which has a convection-diffusion balance followed by a region of thermal explosion which has a balance in reaction, convection, and diffusion.

Figures 18 and 22 depict that as the combustion wave speed or the inflow velocity of the reactant mixture is increased to $v_1 = 20$ m/s, the effects of diffusion start to diminish. In fact, the pre-heat zone of convection-diffusion balance vanishes. The predominant balance is between convection and reaction. Finally, in Figs. 19 and 23, it can be seen that at a combustion wave speed of $v_1 = 100$ m/s, the balance is between reaction and convection only and the diffusion effects become negligible. This is the "fast flame" or "convected explosion" solution.

Note that in this transition from low to high-speed waves, the pressure term and the term representing energy diffusion due to mass diffusion in the energy balance equation remain negligible throughout. However, for wave speeds of the order of 100 m/s, the pressure is not constant, as can be seen in Fig. 2, and the approximate form of the momentum equation must be employed in order to get a self-consistent solution.

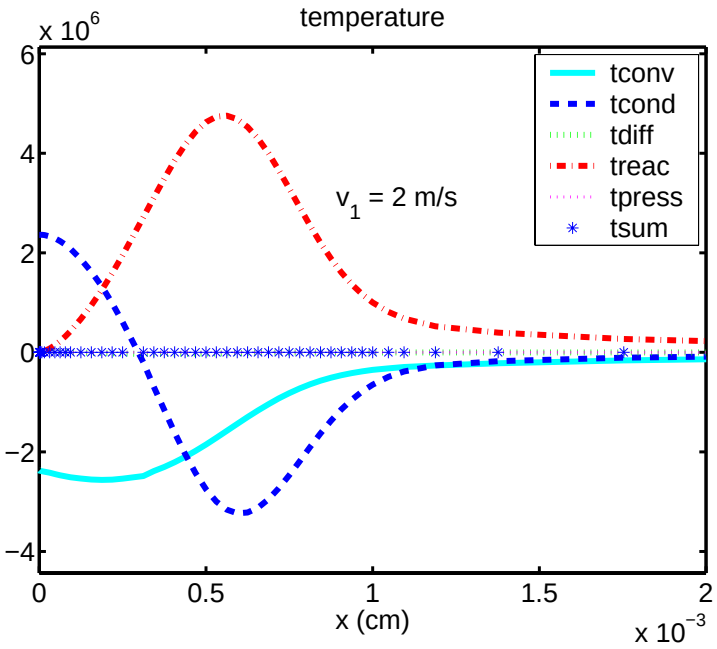

Figure 16: Magnitude of the terms (g-K/cm^3-s) in the energy balance equation for a steady-state stoichiometric methane-air flame. The reactant mixture is at a post-shock state corresponding to a Mach 5 shock, and the inflow velocity of the reactant mixture is 2 m/s.

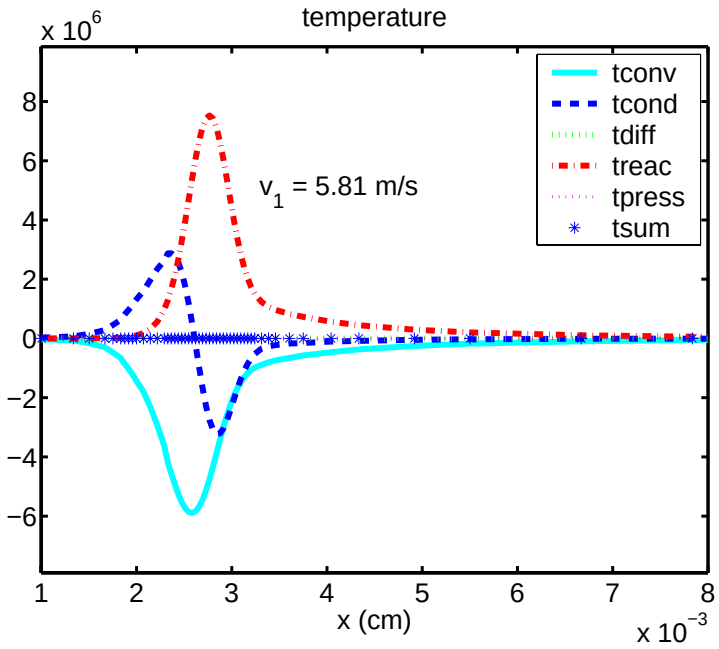

Figure 17: Magnitude of the terms (g-K/cm^3-s) in the energy balance equation for a steady-state stoichiometric methane-air flame. The reactant mixture is at a post-shock state corresponding to a Mach 5 shock, and the inflow velocity of the reactant mixture is 5.81 m/s.

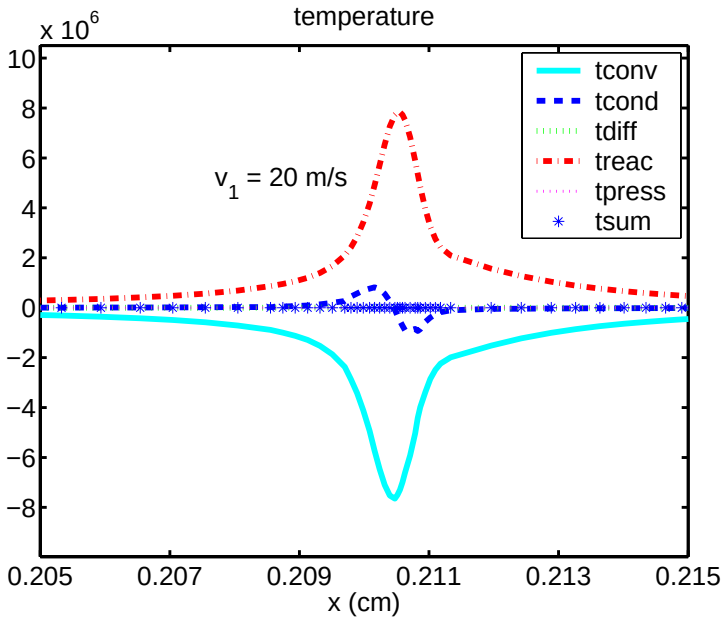

Figure 18: Magnitude of the terms (g-K/cm^3-s) in the energy balance equation for a steady-state stoichiometric methane-air flame. The reactant mixture is at a post-shock state corresponding to a Mach 5 shock, and the inflow velocity of the reactant mixture is 20 m/s.

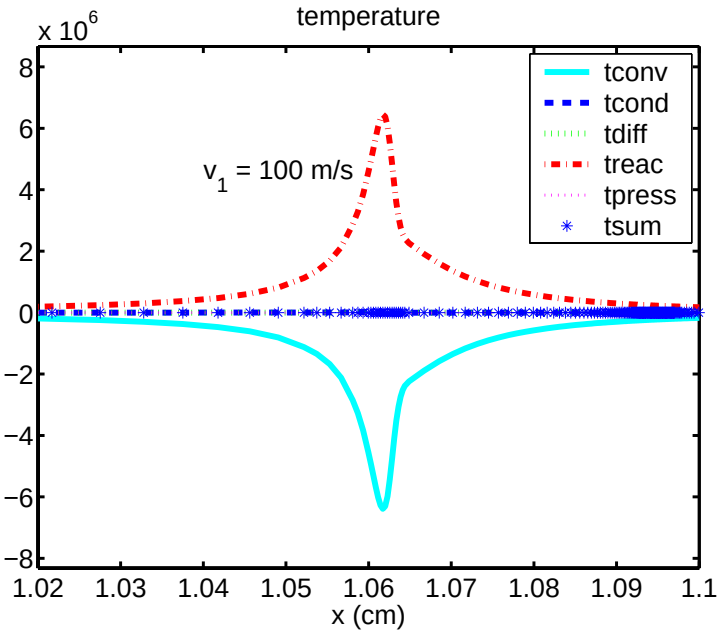

Figure 19: Magnitude of the terms (g-K/cm^3-s) in the energy balance equation for a steady-state stoichiometric methane-air flame. The reactant mixture is at a post-shock state corresponding to a Mach 5 shock, and the inflow velocity of the reactant mixture is 100 m/s.

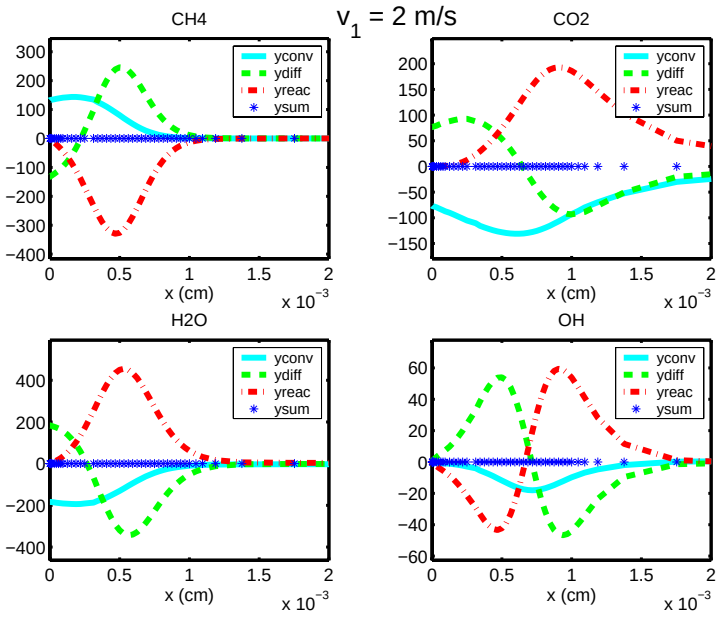

Figure 20: Magnitude of the terms (g/cm^3-s) in the species balance equation for a steady-state stoichiometric methane-air flame. The reactant mixture is at a post-shock state corresponding to a Mach 5 shock, and the inflow velocity of the reactant mixture is 2 m/s.

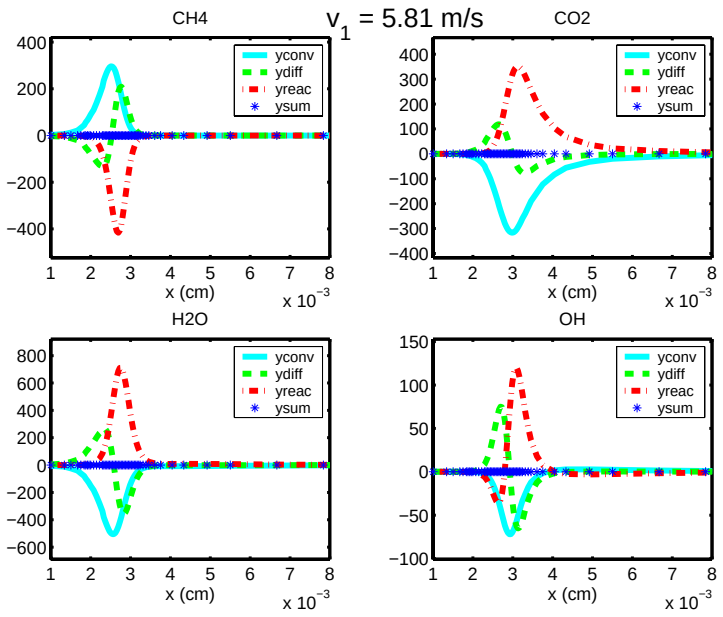

Figure 21: Magnitude of the terms (g/cm^3-s) in the species balance equation for a steady-state stoichiometric methane-air flame. The reactant mixture is at a post-shock state corresponding to a Mach 5 shock, and the inflow velocity of the reactant mixture is 5.81 m/s.

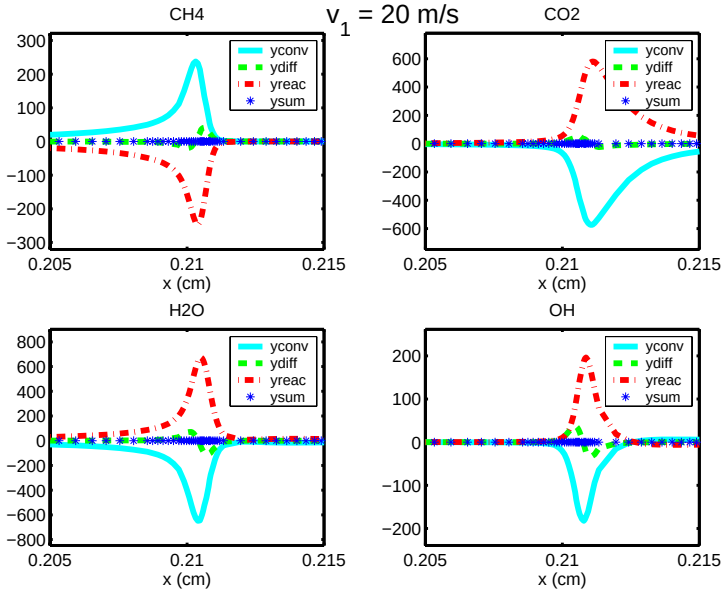

Figure 22: Magnitude of the terms (g/cm^3-s) in the species balance equation for a steady-state stoichiometric methane-air flame. The reactant mixture is at a post-shock state corresponding to a Mach 5 shock, and the inflow velocity of the reactant mixture is 20 m/s.

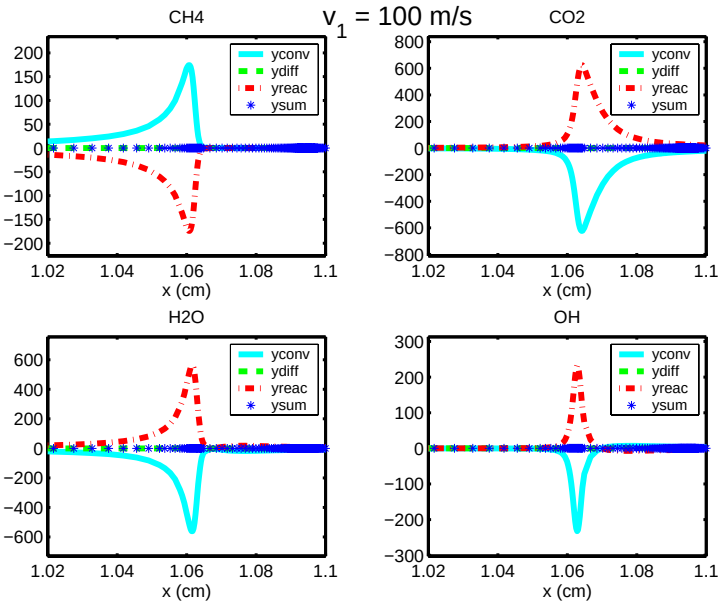

Figure 23: Magnitude of the terms (g/cm^3-s) in the species balance equation for a steady-state stoichiometric methane-air flame. The reactant mixture is at a post-shock state corresponding to a Mach 5 shock, and the inflow velocity of the reactant mixture is 100 m/s.

5.2 Existence of Adiabatic Flame Speed

The results of computing the adiabatic flame speed as a function of shock Mach number are shown in Figs. 9-10 and Table 1. The key to obtaining these results for high post-shock temperatures is to carefully consider the relationship between the inflow conditions and the length where the temperature reaches a specified value. Figure 24 shows the inflow velocity v_1 of the reactant mixture into the steady combustion wave plotted against the length x_{T_1+100} for the case of Mach 4, 5, and 6 shocks. The length x_{T_1+100} is defined as the distance from the inflow computational boundary, in Fig. 13, to the point where the temperature in the combustion wave is 100 K higher than the reactant temperature. On the same plot we have shown with dashed lines the adiabatic constant-pressure explosion distance $x_i = v_1 t_i$, where t_i is the calculated adiabatic explosion induction time, shown in Fig. 11. The length x_i corresponds to the location of the diffusionless combustion wave following a shock of a specified strength. By definition, the induction length increases linearly as the inflow reactant velocity is increased for a fixed shock Mach number. The slope of these lines is the inverse of the induction time t_{T_1+100}, which is defined as the time when the temperature reaches 100 K above the reactant temperature for an adiabatic constant-pressure explosion of the reactants

From Fig. 11 we know that t_{T_1+100} for the shocked reactants decreases as the shock Mach number is increased. Since Fig. 24 is plotted on a log-log scale, the increase in slope of the lines with shock Mach number is not obvious. For a combustion wave where diffusion plays a role,

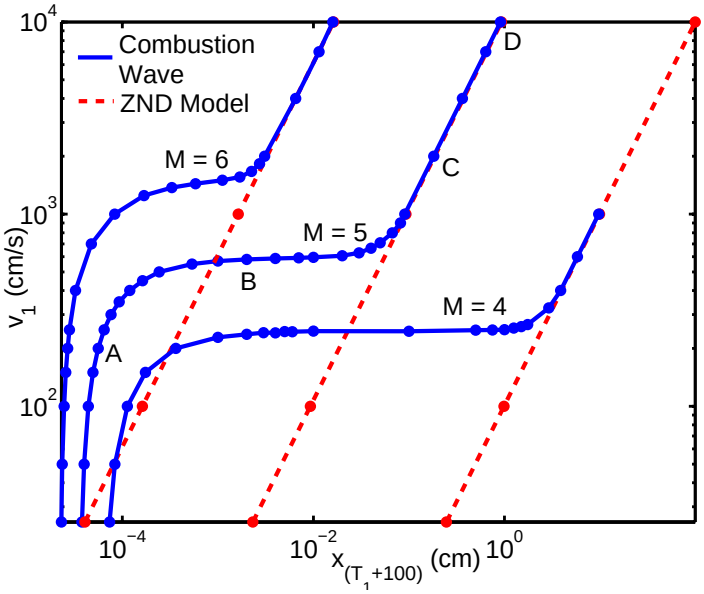

Figure 24: Inflow velocity v_1 of the reactant mixture vs. length x_{T_1+100} for steady-state combustion wave (solid lines) and adiabatic constant-pressure explosion (dashed lines) for stoichiometric methane-air. The plots are for reactant mixture at post-shock states of Mach 4, 5, and 6 shocks.

initially the inflow reactant velocity increases rapidly as the length x_{T_1+100} is increased. Then the value of v_1 levels off at a certain value v_a of the inflow reactant velocity and is independent

of variations in the length x_{T_1+100} for Mach 4 and 5 cases. This plateau value of v_1 is equal the intrinsic adiabatic flame speed v_a for the reactant mixture at that temperature and pressure. In Fig. 24, point A lying on the combustion wave plot for the Mach 5 case corresponds to Figs. 16 and 20, where there is a loss of mass and energy at the inflow computational boundary. There are energy and mass losses at the inflow computational boundary for all inflow velocities below the asymptotic value v_a. In Fig. 24, point B lying on the constant wave speed v_a section of the plot for the Mach 5 case corresponds to Figs. 17 and 21, where there is negligible loss of mass and energy at the left computational boundary. Therefore, point B corresponds to an adiabatic flame.

As the inflow reactant velocity is increased beyond the adiabatic burning velocity v_a, the length x_{T_1+100} asymptotes to the adiabatic explosion distance. In Fig. 24, point C on the plot for the Mach 5 case corresponds to Figs. 18 and 22 and point D corresponds to Figs. 19 and 23. As the length x_{T_1+100} asymptotes to the adiabatic explosion distance, diffusion becomes negligible and the transport balance is only between convection and reaction. The plot for the Mach 4 case is similar to the Mach 5 case. However, for the Mach 6 case, there is not a distinct plateau region and therefore, there is no well-defined adiabatic flame speed. This is because the adiabatic explosion induction distance is so short that it always falls within the flame structure.

Note that when computing the results for Fig. 24, the computations for $v_1 > v_a$ and $v_1 < v_a$ are done using the first mode of the numerical algorithm where the inflow reactant velocity or mass flow rate is fixed. For $v_1 \sim v_a$, we use the second mode of the numerical algorithm where $x_{fix} = x_{T_1+100}$ and $T_{fix} = T_1 + 100$, and the burning velocity is computed as an eigenvalue. The second mode is the most common way of computing the adiabatic flame velocity. However, care should be taken such that x_{fix} lies in the following interval

$$3\delta < x_{fix} < v_a \cdot t_{T_1+100} - \epsilon, \tag{17}$$

where δ is the adiabatic flame thickness and ϵ is an empirically-determined distance which is roughly one-half of the explosion distance. The upper bound for x_{fix} is obvious from Fig. 24 and the lower bound is roughly three times the flame thickness. The size of the interval in Eq. (17) strongly decreases as the reactant temperature or the shock Mach number increases. If x_{fix} is below the lower bound, there will be mass and energy loss at the inflow boundary. If x_{fix} is above the upper bound, the reactant mixture will explode before it reaches x_{fix} and our second mode of computation will predict an erroneously high flame speed.

5.3 Effect of Initial Pressure

In order to investigate whether there exists a condition for which a pure reaction-diffusion balance exists in the latter part of the flame, pre-mixed adiabatic flames were computed for a stoichiometric methane-air mixture at a temperature of 300 K but with increasing pressure. It can be seen by comparing Figs. 25 and 26 that the convection effects are reduced in the downstream region of the flame as the pressure of the reactant mixture is increased. However, even at a pressure of 100 atm, the convection contribution remains finite. This is even more apparent in comparing Fig. 27 and 28 for the terms in the species transport equations. This effect persists even when we do the computations for higher pressures. The computed flame speeds decrease with increasing initial pressure as shown in Fig. 29 and Table 2. The variation of flame speed with initial pressure is consistent with the data (Gaydon and Wolfhard, 1979) and the results of previous studies (Frenklach et al., 1995) using this chemical reaction mechanism.

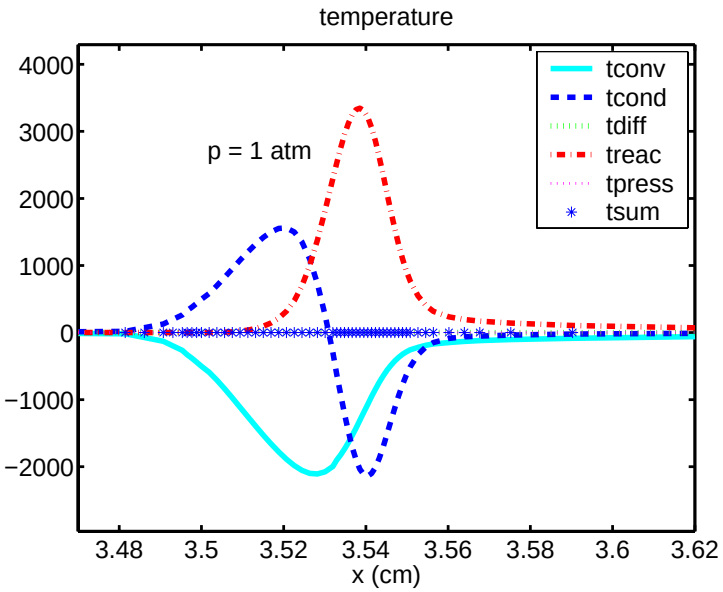

Figure 25: Magnitude of the terms (g-K/cm^3-s) in the energy balance equation for an adiabatic stoichiometric methane-air flame. The reactant mixture temperature and pressure are 300 K and 1 atm, respectively.

We conclude that the separation of the flame into distinct convection-diffusion and reaction-diffusion zones is a useful pedagogical tool but does not occur in practice for the conditions we have examined.

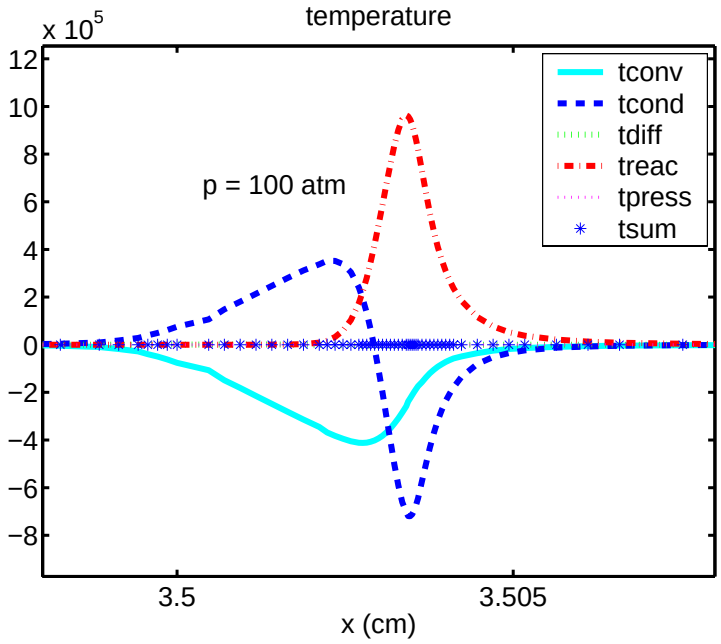

Figure 26: Magnitude of the terms (g-K/cm^3-s) in the energy balance equation for an adiabatic stoichiometric methane-air flame. The reactant mixture temperature and pressure are 300 K and 100 atm, respectively.

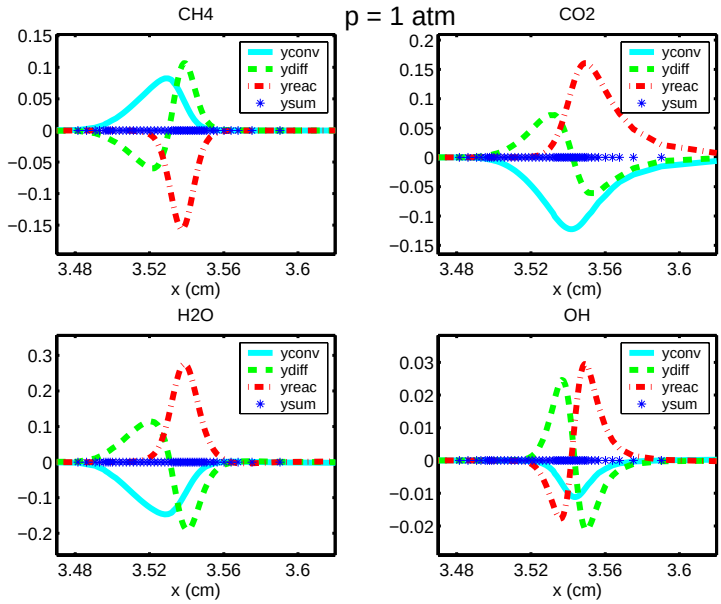

Figure 27: Magnitude of the terms (g/cm^3-s) in the species balance equation for an adiabatic stoichiometric methane-air flame. The reactant mixture temperature and pressure are 300 K and 1 atm, respectively.

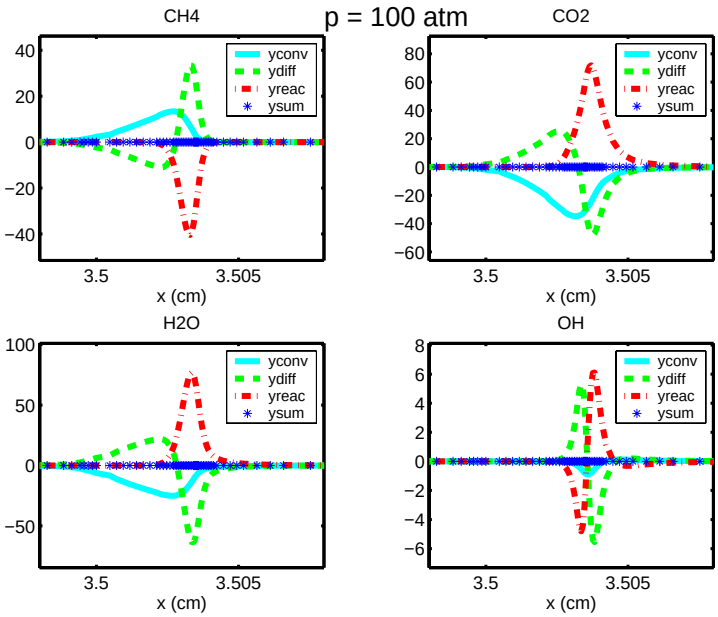

Figure 28: Magnitude of the terms (g/cm^3-s) in the species balance equation for an adiabatic stoichiometric methane-air flame. The reactant mixture temperature and pressure are 300 K and 100 atm, respectively.

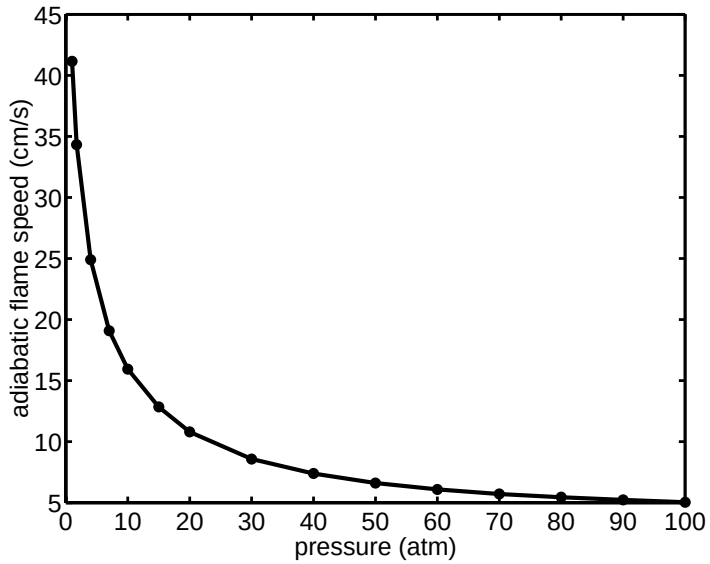

Figure 29: Adiabatic flame speed vs. reactant pressure for a reactant mixture of stoichiometric methane-air at a temperature of 300 K.

6 Conclusions

There are two key conclusions from our work. First, the role of diffusion appears to be negligible for one-dimensional combustion waves with speeds over 20 m/s for an initial condition corresponding to the state behind a Mach 5 shock. This observation is, as expected, in complete agreement with the analysis of Clarke (1989) and quantifies this effect. A combustion wave speed of 20 m/s corresponds to a Mach number of 0.003 at this state (T_1 = 1491 K, c_1 = 752 m/s). This indicates that, for all practical purposes, one-dimensional analyses of spontaneous flames (Zel'dovich, 1980) created by induction time gradients (Gu et al., 2003) can be analyzed by neglecting diffusive processes in laboratory situations where the wave speeds are usually greater than 100-200 m/s. In particular, the role of diffusive transport in the classical one-dimensional (steady) detonation solution can be definitely ruled out. Second, the notion of adiabatic flame speed is well-defined only as long as there can be a clear separation in scales between the induction length and flame pre-heat length. For our examples, this is possible as long as the leading shock Mach number is less than or equal to 5. Beyond this, the pre-heat and induction zones merge and it is not possible to have a unique burning speed. The maximum value of the burning speed behind a Mach 5 shock is predicted to be 5.8 m/s, about 50 times slower than the fluid velocity relative to the shock wave, 300 m/s. It appears that adiabatic flames are marginally possible behind strong shock waves with propagation speeds (M = 5.11) comparable to detonations in stoichiometric methane-air mixtures. Clearly, this will have to be investigated for a range of compositions before it can be generalized.

Accepting that there is a regime where adiabatic flames may exist behind strong shock waves, we can make some speculations about the relevance of this to detonation propagation mechanisms. In a multi-dimensional situation such as observed behind highly unstable detonation waves, the combustion front can be substantially distorted (Pintgen et al., 2003, Austin, 2003) by the spatial non-uniformity and temporal oscillations in the leading shock strength, see Fig. 30. Although our study shows that diffusion is negligible for steady one-dimensional detonations or one-dimensional high speed combustion waves following shocks, diffusively-controlled combustion may still play a role in these highly unstable detonation fronts. This is because the actual situation is multidimensional and unsteady, opening up the possibility that the combustion process may be highly anisotropic with diffusion transverse to the main propagation direction playing a role in these unstable fronts. It is also known Austin (2003) that the unsteadiness of the shock fronts in these unstable waves can substantially alter the explosion times, creating an essentially unsteady situation in which temporally developing diffusion layers may play a role.

Building on the simple turbulent flame notions of Damköhler (Peters, 2000, see pp. 119-121), this suggests that the effective combustion front area (Liñán and Williams, 1993, see p. 127-131) will then have to be of the order of 50, which is the ratio of the bulk gas velocity to the laminar burning speed, if diffusive processes are to be effective in contributing to the combustion rate. In low-speed turbulent pre-mixed flames, the ratio of turbulent to laminar burning velocity can be up to a factor of 15 (Peters, 2000, see Fig. 2.22) at high turbulence intensities. Additional surface area can be produced by large-scale motions, i.e., the organized structures observed in shear layers or, in the case of detonations, the motion induced by the quasi-periodic cellular instability. Therefore, the role of diffusive processes behind multi-dimensional (unsteady) detonations cannot be conclusively ruled out on the basis of the present study. Clearly, this idea is at an early stage and much work needs to be done in both analyzing the experimental data

and shoring up the theoretical arguments.

Acknowledgments

This work is supported by the DOE ASCI/ASAP Center of Excellence at the California Institute of Technology and the Office of Naval Research. We thank F. Pintgen for providing the images shown in Fig. 30.

References

G. E. Andrews and D. Bradley. Determination of burning velocity; a critical review. *Combust. Flame.*, 18:133–, 1972.

Joanna Austin. *The Role of Instability in Gaseous Detonation*. PhD thesis, California Institute of Technology, Pasadena, California, June 2003.

G. Q. Chen and D. H. Wagner. Global entropy solutions to exothermically reacting, compressible euler equations. *J Differ Equations*, 191(2):277–322, July 2003.

J. F. Clarke. Fast flames, waves and detonation. *Progress In Energy and Combustion Science*, 15(3):241–271, 1989.

John F. Clarke. On the changes in structure of steady plane flames as their speed increases. *Combust. Flame*, 50:125–138, 1983.

M. Elia, M. Ulinski, and M. Metghalchi. Laminar burning velocity of methane-air-diluent mixtures. *J. Eng. Gas Turbines and Power, Transactions of the ASME*, 123:190–196, 2001.

W. Fickett and W. C. Davis. *Detonation*. University of California Press, Berkerely, CA, 1979.

M. Frenklach, H. Wang, C.-L. Yu, M. Goldenberg, C.T. Bowman, R.K. Hanson, D.F. Davidson, E.J. Chang, G.P. Smith, D.M. Golden, W.C. Gardiner, and V. Lissianski. GRI Mech 1.2. http://www.me.berkeley.edu/gri_mech/, 1995.

A. M. Garforth and C. J. Rallis. Laminar burning velocity of stoichiometric methane-air - pressure and temperature dependence. *Combust. Flame*, 31:53–68, 1978.

A. G. Gaydon and H. G. Wolfhard. *Flames, their structure, radiation, and temperature*. Chapman and Hall, fourth edition, 1979.

X. J. Gu, D. R. Emerson, and D. Bradley. Modes of reaction front propagation from hot spots. *Combust. Flame*, 133:63–74, 2003.

P. G. Hill and J. Hung. Laminar burning velocities of stoichiometric mixtures of methane with propane and ethane additives. *Combust. Sci. Technol.*, 60:7–30, 1988.

R. J. Kee, G. Dixon-Lewis, J. Warnatz, M. E. Coltrin, and J. A. Miller. A FORTRAN computer code package for the evaluation of gas-phase multicomponent transport properties. Technical Report SAND86-8246, Sandia National Laboratories, 1986.

R. J. Kee, J. F. Grcar, M. D. Smooke, and James A. Miller. A FORTRAN program for modeling steady laminar one-dimensional premixed flames. Technical Report SAND85-8240, Sandia National Laboratories, 1985.

R. J. Kee, F. M. Rupley, and James A. Miller. The CHEMKIN thermodynamic data base. Technical Report SAND87-8215, Sandia National Laboratories, 1987.

R. J. Kee, F. M. Rupley, and James A. Miller. CHEMKIN-II: A Fortran chemical kinetics package for the analysis of gas-phase chemical kinetics. Technical Report SAND89-8009, Sandia National Laboratories, 1989.

R.J. Kee, M. E. Coltrin, and P. Glarborg. *Chemically reacting flow: theory and practice*. Wiley, 2003.

R. Knystautas, J.H.S. Lee, J. E. Shepherd, and A. Teodorczyk. Flame acceleration and transition to detonation in benzene-air mixtures. *Combustion and Flame*, 115:424–436, 1998.

A. Liñań and F. A. Williams. *Fundamental Aspects of Combustion*. Oxford University Press, 1993.

D. P. Mishra. Effects of initial temperature on the structure of laminar diffusion flames. *Fuel*, 82:1471–1475, 2003.

Norbert Peters. *Turbulent Combustion*. Cambridge University Press, 2000.

L. R. Petzold. A description of DASSL: a differential/algebraic system solver. Technical Report SAND82-8637, Sandia National Laboratories, 1982.

F. Pintgen, J. M. Austin, and J. E. Shepherd. Detonation front structure: Variety and characterization. In G.D. Roy, S.M. Frolov, R.J. Santoro, and S.A. Tsyganov, editors, *Confined Detonations and Pulse Detonation Engines*, pages 105–116. Torus Press, Moscow, 2003.

W. C. Reynolds. The element potential method for chemical equilibrium analysis: implementation in the interactive program STANJAN. Technical report, Stanford University, 1986.

S. Singh, Y. Rastigejev, S. Paolucci, and J. M. Powers. Viscous detonation in H_2-O_2-Ar using intrinsic low-dimensional manifolds and wavelet adaptive multilevel representation. *Combustion Theory and Modelling*, 5(2):163–184, June 2001.

R. Stone, A. Clarke, and P. Beckwith. Correlation for laminar burning velocity of methane/diluent/air mixtures obtained in free-fall experiments. *Combust. Flame*, 114:546–555, 1998.

W. G. Vincenti and C. H. Kruger. *Introduction to Physical Gas Dynamics*. Wiley, 1965.

Y. B. Zel'dovich. Regime classification of an exothermic reaction with nonuniform initial conditions. *Combust. Flame*, 39(2):211–214, 1980.

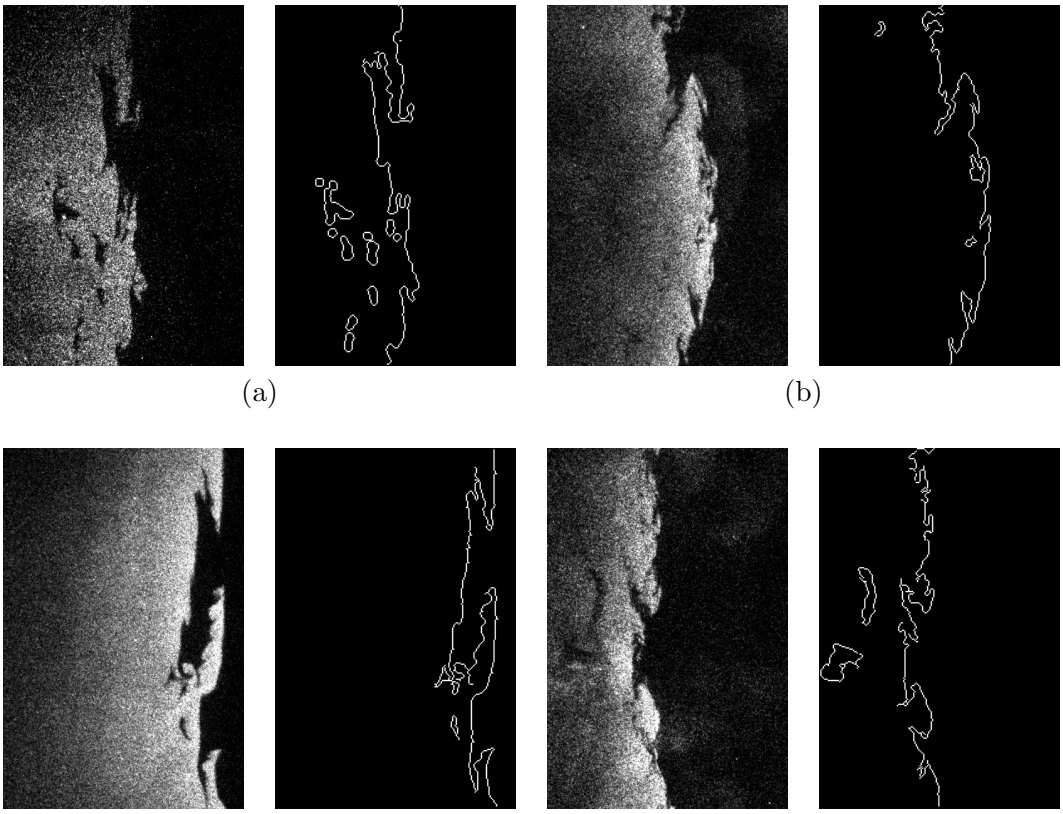

Figure 30: PLIF images and derived OH fronts. Previously unpublished images obtained as part of the study by Pintgen et al (2003). Case a: 0.588 N_2, 0.235 H_2, 0.118 N_2O, 0.059 O_2, P = 11.3 kPa, 51 mm image height. Case b: 0.50 N_2, 0.25 H_2, 0.25 N_2O, P = 30.4 kPa, 30 mm image height. Case c: 0.588 N_2, 0.235 H_2, 0.118 N_2O, 0.059 O_2, P = 30.4 kPa, 30 mm image height. Case d: 0.50 N_2, 0.25 H_2, 0.25 N_2O, P = 30.4 kPa, 30 mm image height.

A Tabular Data

M	U_{shock} (m/s)	T_1 (K)	P_1 (atm)	v_a (m/s)	δ (μm)
1.0	354	300	1.00	0.411	425
1.5	531	393	2.47	0.481	194
2.0	708	496	4.53	0.591	111
2.5	885	619	7.21	0.787	68.8
3.0	1062	760	10.5	1.120	44.4
3.5	1239	918	14.4	1.630	29.5
4.0	1416	1092	19.0	2.500	20.1
5.0	1770	1489	30.0	5.810	9.90
6.0	2124	1949	43.5		5.40

Table 1: Post-shock conditions T_1, P_1, adiabatic flame speeds v_a, and flame thickness δ as a function of shock Mach number M or shock velocity U_{shock} for stoichiometric methane-air mixtures.

P (atm)	v_a (m/s)
1	0.411
1.75	0.343
4	0.249
7	0.191
10	0.160
15	0.128
20	0.108
30	0.0859
40	0.0739
50	0.0661
60	0.0610
70	0.0572
80	0.0545
90	0.0523
100	0.0505

Table 2: Adiabatic flame speed v_a as a function of initial pressure P for stoichiometric methane-air mixtures at an initial temperature of 300 K.

Mach number	induction time (s)
3.25	7.84×10^{-1}
3.50	1.45×10^{-1}
3.75	3.53×10^{-2}
4.00	9.89×10^{-3}
4.25	2.93×10^{-3}
4.50	8.99×10^{-4}
4.75	2.84×10^{-4}
5.00	9.28×10^{-5}
5.25	3.15×10^{-5}
5.50	1.13×10^{-5}
5.75	4.35×10^{-6}
6.00	1.82×10^{-6}
6.25	8.27×10^{-7}
6.50	4.07×10^{-7}
6.75	2.16×10^{-7}
7.00	1.22×10^{-7}

Table 3: Adiabatic homogeneous explosion time (constant pressure model) behind shock waves as a function of shock Mach number for stoichiometric methane-air mixtures at an initial temperature of 300 K. The induction times correspond to the temperature increase of 100 K over the initial value.

B Scaling Analysis of Species Equation

The steady state species transport equation (5) can be written in simplified form for a single mass fraction Y as

$$\underbrace{v\frac{dY}{dx}}_{\text{Conv}} - \underbrace{D\frac{d^2Y}{dx^2}}_{\text{Diff}} - \underbrace{\frac{\dot{\omega}W}{\rho}}_{\text{Reac}} = 0 \tag{18}$$

where we have labeled the terms according to their roles. The goal of our analysis is to use simple physically-based estimates of the magnitude of each term in order to determine the relative size of each contribution to the transport equation. In doing so, we follow ideas of Clarke (1989) in choosing the reference quantities that enter into the scaling.

The basic scaling quantities are the reference velocity U, which we chose to be the combustion wave velocity, the length scale δ that characterizes the width of the spatial gradient region, and the chemical reaction time scale t_{chem}. The mass fraction Y is dimensionless and considered to be of order one in size. In terms of these reference quantities, we can estimate the size of each term as

$$\begin{aligned} v\frac{dY}{dx} &\sim U/\delta \,, \\ D\frac{d^2Y}{dx^2} &\sim D/\delta^2 \,, \\ \frac{\dot{\omega}W}{\rho} &\sim \frac{1}{t_{chem}} \,, \end{aligned}$$

and note that each of these has the dimensions of a reciprocal time. The principle of dominant balance means that for there to be a nontrivial solution, at least two of the three terms must be of comparable size at each point within the reaction zone. The chemical reaction time scale is the reciprocal of the normalized reaction rate and is, therefore, a strong function of temperature. This means that the dominant balance may vary with position within the combustion wave as the temperature changes during the course of the reaction. Another interpretation is that the time scales for two of the three processes must be comparable in this equation. A concise measure of the relative time scale of flow processes (convection and diffusion) as compared to chemical processes (reaction) is the Damköhler number

$$Da = \frac{t_{flow}}{t_{chem}} \,. \tag{19}$$

The Damköhler number is necessarily a strong function of position within a flame since the temperature varies with position and the reaction time will also.

Low-Speed (Diffusion-Controlled) Combustion Waves

Low-speed diffusion-controlled flames are distinguished by having a sufficiently low temperature upstream that there is a "pre-heat" zone in which the reaction is negligible. This is followed by a thin (usually about 1/10 the width of the pre-heat zone) main reaction zone in which reactants are converted to products and chemical energy is converted to thermal. Within the pre-heat zone, convection is balanced by diffusion, with products and reactive intermediates

diffusing upstream from the main reaction region and causing ignition of the cold reactants. By estimating the thickness of the pre-heat zone and balancing energy and species fluxes upstream with the generation rate within the main reaction layer, we can develop estimates for the flame thickness and speed. We present a very simplified version of this below; the details can be found in any combustion text, for example, Liñán and Williams (1993, pp. 22-32).

Convection-Diffusion Balance

Consider a situation in which the upstream temperature is low enough that the reaction rate is negligible and only the convection and diffusion terms can contribute to the transport. This corresponds to the limit of $Da \to 0$, very slow reaction. The approximate species equation will be

$$v\frac{dY}{dx} - D\frac{d^2Y}{dx^2} \approx 0 \tag{20}$$

which, if the reaction zone is located at x =0, will have the solution

$$Y(x) = Y(0)\exp(xU/D) \qquad x < 0 \tag{21}$$

for a species which has zero concentration far upstream in the reactant region and a constant flow velocity $v = U$. This solution shows that the characteristic thickness of the convection-diffusion zone is $\delta = D/U$ which agrees with a dominant balance between convection and diffusion, for which we have

$$U/\delta \sim D/\delta^2 \, . \tag{22}$$

Diffusion-Reaction Balance

At the downstream end of the diffusion zone, the temperature is high, and if the reaction zone region is thin, then the reaction term must be balanced by diffusion alone. This implies that the chemical reaction rate is such that the Damköhler number is of order one. Equating our estimates of the size of these terms and using the previous result for the thickness of the diffusion zone, we have

$$\frac{U^2}{D} \sim \frac{1}{t_{chem}} \tag{23}$$

which leads to the standard estimate for adiabatic flame speed of

$$U \sim \sqrt{\frac{D}{t_{chem}}} \, . \tag{24}$$

A similar analysis can be made of the energy equation (Liñán and Williams, 1993), with the thermal diffusivity κ replacing the species diffusivity. The ratio of the diffusivities, $Le = \kappa/D$, is the Lewis number and determines the relative width of the thermal and species profiles. A quantitative analysis of the propagation velocity must proceed more carefully, including the Lewis number and also the reduced activation energy as parameters (Liñán and Williams, 1993).

High-Speed (Diffusionless) Combustion Waves

High-speed combustion waves are characterized by having a sufficiently high reactant temperature that diffusion is not needed in order to get ignition of the reactants. Unlike low-speed diffusion-controlled waves, the combustion wave speed is not an eigenvalue of the adiabatic reaction equations but is determined by the initial conditions. These initial conditions are usually in the form of a specified temperature and reactant profile. A physical mechanism for producing temperature gradients is often taken to be an unsteady shock wave generated externally to the problem.

The key to the scaling analysis of high-speed combustion is to choose a length scale that is based on the local induction time, i.e., the adiabatic explosion time associated with the reactant temperature, pressure, and composition. We will proceed by assuming that, in high-speed combustion the dominant balance is between convection and reaction, justifying this choice a posteriori. We will then show how to estimate the size of the diffusion term and how the relative contributions of diffusion and reaction depend on the combustion wave speed. To do this precisely requires a more subtle treatment (Clarke, 1989) and the treatment here is heuristic.

Convection-Reaction Balance

In high-speed combustion, the length scale is the induction length $\delta = Ut_i$, where t_i is the adiabatic explosion time. The adiabatic explosion time is the characteristic chemical reaction time for this case, as can be seen by equating the estimates for the convection and reaction terms.

$$\frac{U}{\delta} \sim \frac{1}{t_{chem}} \qquad \text{or} \qquad \delta \sim U t_{chem} \tag{25}$$

With this choice of the length scale, convection and reaction will automatically be in balance.

Magnitude of Diffusion Contribution in High-Speed Waves

Using the length scale based on the induction time, the ratio of the diffusion term to the reaction term can be computed to be

$$\frac{\text{Diff}}{\text{Reac}} \sim \frac{D}{U^2 t_{chem}} \, . \tag{26}$$

This can be further simplified by using the Clarke (1989) estimate for reaction rate. Clarke suggests modeling the reaction time as being proportional to the collision time with a multiplicative factor $R(T, \rho, Y)$ accounting for the temperature, density, and composition dependence of the reaction rate. Approximating the collision time using the diffusivity and sound speed (Vincenti and Kruger, 1965, p. 19), we get

$$\frac{1}{t_{chem}} = \frac{c^2}{D} R(T, \rho, Y) \tag{27}$$

where c is the frozen sound speed. Using this representation, we find that

$$\frac{\text{Diff}}{\text{Reac}} \sim \frac{C^2}{U^2} R(T, \rho, Y) = \frac{1}{Ma^2} R(T, \rho, Y) \tag{28}$$

where $Ma = U/c$ is the Mach number of the combustion wave. We conclude that, all other factors being the same, the diffusion term will scale as $1/Ma^2$ times the reaction term in high-speed combustion waves. This is verified by examining the results for the shock Mach 5 case shown in Figs. 17-19; the ratio of diffusion-to-reaction terms decreases from 0.6 at the adiabatic combustion wave speed of 5.8 m/s to 0.10 at 20 m/s, and to less than .005 at 100 m/s, see Fig. 31. For the CJ detonation case, the relative contribution of diffusion to the energy equation is less than 0.0005.

We conclude that the scaling results of Clarke are verified in our numerical simulations and that the role of diffusion in high-speed (combustion wave speeds greater than 20 m/s) one-dimensional flames and detonations is negligible.

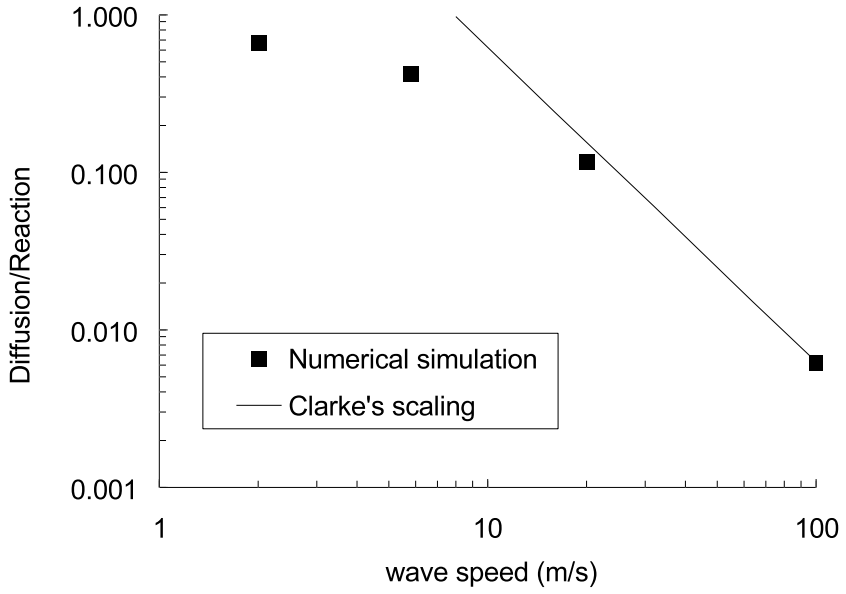

Figure 31: Ratio of diffusive transport terms to reaction term in energy equation for combustion waves with speeds between 2 and 100 m/s, initial conditions correspond to post-shock values for $M = 5$ shock.